Unifying Distributed Dynamic Optimization and Control of Islanded DC Microgrids

Seyedali Moayedi and Ali Davoudi, *Senior Member, IEEE*

***Abstract*—A distributed control method is proposed to simultaneously optimize the power sharing among sources of islanded dc microgrids, while regulating the distribution bus voltage. During the optimization process, an economic dispatch problem is solved to minimize the total generation cost by setting the output powers of the dispatchable sources. To this end, the voltage set points of individual dc–dc converters are adjusted using a voltage regulator and an optimizer, which regulates the average voltage of the sources to establish the generation–consumption equality constraint and matches the incremental costs, respectively. Afterward, the proposed optimizer is modified to exclude the sources from the incremental cost consensus protocol upon reaching their generation limits, enforcing inequality constraints. This coregulation and cooptimization paradigm is developed in a fully distributed fashion. The dynamical model of the proposed controller is established. The steady-state analysis verifies the fulfillment of the control objectives, i.e., voltage regulation and cost minimization. Experimental results verify the controller performance and validate its resiliency against cyber and physical faults.**

***Index Terms*—Cooperative control, dc microgrids, graph theory, optimization.**

I. Introduction

THIS paper provides a fully distributed control-theoretic framework for simultaneous dynamic voltage regulation and optimal resource utilization of islanded dc microgrids. The U.S. Department of Energy defines microgrids a group of interconnected loads and distributed energy resources with clearly defined electrical boundaries that acts as a single controllable entity with respect to the grid [1]. Multiconverter dc distribution networks, also commonly referred to as islanded dc microgrids, are increasing in popularity as they offer an efficient and reliable power delivery platform accommodating dc-native emerging resources (e.g., photovoltaic), loads (e.g., electronic loads, electric vehicle chargers, and LED lighting), and storage elements (e.g., batteries) [2]–[5]. Islanded mode of operation creates unique control challenges that have recently received significant attention (e.g., [6]–[13]). The decision-making objectives in an islanded dc microgrid are to ensure operational stability, synchrony, and optimality [14]–[17]. Such objectives are achieved, respectively, using load sharing [18], [19], voltage regulation [2], [20], [21], and minimizing the operating costs or losses [22]–[24]. While load sharing and voltage regulation of islanded dc microgrids have been studied in detail (e.g., [25]–[29]), the optimization frameworks, particularly economic dispatch of resources, have not received proper considerations. In addition, optimal operation and voltage regulation/load sharing are conventionally managed at different temporal scales. Finally, such decision-making tasks are handled by a central entity, which exposes a single point of failure and limits expandability. Since islanded dc microgrids are increasingly utilized in resource-constrained safety/mission-critical application domains, e.g., electric ships [30]–[41], electric aircraft [42]–[46], or forward operating bases [47], optimal utilization of limited resources, while using a resilient distributed decision-making process, is of paramount value [48]–[53].

Although economic dispatch of ac transmission systems is a classic concept [54], [55], its extension to dc microgrids is very recent. The load demand must be carefully dispatched among dc sources so as to minimize the total generation cost, all while respecting the generation capacity of dc sources. Quadratic cost functions of converter-augmented (dispatchable) dc sources, with generation–demand equality and generational-limit inequalities, are considered. The renewable resources, e.g., wind and solar, are considered nondispatchable and excluded from the problem formulation as they are desired to produce the maximum power. The optimization problem in dc microgrids has been addressed from different perspectives in the literature. For example, Meng, Dragicevic, Guerrero, and Vasquez [24] have optimized the global efficiency of a dc microgrid by adjusting droop gains. Economic dispatch in [56] dynamically tunes droop coefficients to generate power from less costly sources. In [23], the total system cost, including initial, operational, and maintenance costs, is optimized. Linear and dynamic programming approaches in [57]–[59] schedule microgrid operation at hour (or day-ahead) timescales. The focus of this paper, in contrast, is on real-time voltage control and resource optimization.

Structurally, dc microgrids can be controlled in a centralized [15], [60], decentralized [61], [62], or distributed fashion [18], [63]. Centralized controllers expose a single point of failure, are prone to modeling error, suffer from the curse of dimensionality, and lack flexibility and expandability. Decentralized control methods, e.g., droop mechanisms, are more reliable and modular. However, exchange of information, even limited, ensures that converters share a common control objective and adequately adapt to the changes in global information. Therefore, decentralized methods alone cannot guarantee optimal operation of

Manuscript received June 4, 2015; revised February 15, 2016; accepted May 3, 2016. Date of publication May 10, 2016; date of current version December 9, 2016. This work was supported in part by the National Science Foundation under Grant ECCS-1405173 and by the U.S. Office of Naval Research under Grant N00014-14-1-0718. Some initial findings of this work were presented at the 2015 IEEE Workshop on Control and Modeling for Power Electronics. Recommended for publication by Associate Editor B. Lehman.

The authors are with the Department of Electrical Engineering, University of Texas, Arlington, TX 76019 USA (e-mail: seyedali.moayedi@mavs.uta.edu; davoudi@uta.edu).

Color versions of one or more of the figures in this paper are available online at http://ieeexplore.ieee.org.

Digital Object Identifier 10.1109/TPEL.2016.2565517

dc microgrids [18], [64], [65]. Distributed methods combine the useful features of both centralized and decentralized approaches using asynchronous information exchange via sparse communication with neighbor converters. This improves the reliability and scalability, compared to centralized controllers, and system performance, compared to decentralized controllers [66], [67]. Although distributed control of dc microgrids has garnered significant attention lately (e.g., [14], [18], [63], [68], [69]), distributed optimization paradigms are yet to be explored for dc microgrid applications. An exception is [64] that uses dynamic consensus protocols to propagate the system-wide efficiency information to minimize microgrid losses.

From a temporal perspective, real-time coordination and steady-state optimization problems are usually handled on different timescales. Often slower and iterative optimization process provides the reference point for real-time control [59], [70]. Such limiting assumptions are recently challenged in inverter-based ac microgrids [71]–[73] or bulk ac power systems [74]–[76]. However, the temporal gap between the optimality (e.g., economic dispatch of dc resources) and synchrony (e.g., voltage regulation) has not yet been bridged for multiconverter dc microgrids. Accordingly, this paper unifies the voltage regulation and resource optimization frameworks of a dc microgrid, in a fully distributed fashion, such that the voltage set points to regulate dc bus voltages seek the solutions to the economic dispatch of dispatchable dc resources. This is achieved using distributed consensus protocols on incremental costs of dc resources, that are defined as the slope of cost functions [25], and properly incorporating such incremental costs in voltage controllers embedded in individual converters networked on a communication graph. The salient contributions of this paper are as follows.

1) The voltage control module of each dc–dc converter is augmented with an additional voltage regulator and an optimizer, both running local voting protocols to adjust the corresponding voltage set points. While the optimizer minimizes the total generation cost by having the incremental costs of all the sources reach a consensus, another protocol is run in the voltage regulator to tune the average voltage of the sources to the desired voltage set point.
2) The coordination and optimization process happen simultaneously, which allows for the online optimization if the cost functions or power limits of the sources change. Moreover, the voltage controller simultaneously fulfills the generation–demand equality constraint in the optimization process.
3) The proposed framework is fully distributed; converters share only the voltage and incremental cost information with their neighbors on a sparse communication network.
4) The proposed controller offers resiliency against any failure in sources, converters, or communication links so long as the graph of the remaining communication network features a spanning tree. In addition, there is no need for *a priori* knowledge (or knowledge update for) the number of sources and their power limits. Therefore, the controller provides a plug-and-play platform for participating sources. The proposed method is leaderless, i.e., it does not rely on a leader node, which could jeopardize a solution's configurability and pose reliability concerns if the leader node is compromised.

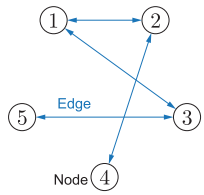

Fig. 1. Graphical representation of a distributed system with five active agents.

The rest of this paper is outlined as follows. Section II explicates the graph theory and its applications in distributed control systems. In Section III, the optimization problem is formulated. Section IV unifies the distributed optimization and real-time control paradigms. The system-level model, including the converter models, power distribution network, controller/optimizer, and communication network, is developed in Section V. The steady-state analysis is provided in Section VI. The optimization and coordination paradigms are verified on a dc microgrid prototype in Section VII. Section VIII concludes the paper.

II. Cooperative Control Framework: Interaction on Graphs

In a distributed control paradigm, the control agents exchange data through a communication network. Graph theory is used for graphical representation of the communication network in multiagent systems [29], [77]–[80]. As shown in Fig. 1, a graph is composed of a set of nodes, $\{\nu_1, \ldots, \nu_N\}$, and a set of edges, which represent control agents and communication links, respectively. An edge connects a node to another node (i.e., its neighbor). The set of all neighbors of the node ν_i is represented by N_i. In a directed graph, the edge directions indicate the direction of information flow. The information exchange process in a directed graph is not reciprocal, i.e., $\nu_j \in N_i$ does not guarantee that $\nu_i \in N_j$. A graph with N nodes can be represented by an adjacency matrix

$$\mathbf{A} = [a_{ij}] \in \mathbb{R}^{N\times N}. \tag{1}$$

The adjacency matrix represents the communication structure; $a_{ij} > 0$, if there is an edge from node ν_j to node ν_i, and $a_{ij} = 0$ otherwise. The diagonal in-degree matrix is $\mathbf{D} = [d_{ij}] \in \mathbb{R}^{N\times N}$, where d_{ii}, the in-degree of the node ν_i is defined as the row-sum of the ith row of the adjacency matrix

$$d_{ii} = \sum_{j=1}^{N} a_{ij}. \tag{2}$$

Then, the Laplacian matrix is defined as $\mathbf{L} = \mathbf{D} - \mathbf{A}$ with all row-sums equal to zero

$$\mathbf{L}\begin{bmatrix}1 \ldots 1\end{bmatrix}^{\mathrm{T}} = 0. \tag{3}$$

The out-degree of the node ν_i is defined as the column-sum of the ith column of the adjacency matrix. If the number of in-degrees and out-degrees are equal for each node, the Laplacian matrix has all the row-sums and column-sums equal to zero

and is said to be balanced. The Laplacian matrix has a zero eigenvalue, e.g., λ_1, with the corresponding eigenvector $v_1 = [1 \ \dots \ 1]^{\mathrm{T}}$. A directed path is defined as a sequence of nodes $\{\nu_1, \dots, \nu_r\}$, where there is a node from ν_i to ν_{i+1} for every i from 1 to $r-1$. A graph is said to have a spanning tree if it contains a node, called the root node, which has at least one direct path to all other nodes. If a graph has a spanning tree, $\lambda_1 = 0$ is a nonrepeated eigenvalue, $\mathrm{rank}(\mathbf{L}) = N-1$, and the only solution to $\mathbf{Lx} = \mathbf{0}$ is $\mathbf{x} = c[1 \ \dots \ 1]^{\mathrm{T}}$, where c is a constant. In the synchronization problem discussed in this paper, the control agents are designed to hold $\mathbf{Lx} = \mathbf{0}$ at the steady state, where $\mathbf{x} = [x_1 \ \dots \ x_N]^{\mathrm{T}}$ is a global vector. This forces all the x_is to reach a consensus at the steady state.

III. Optimization Problem Definition

Optimizing the microgrid performance is considered from minimizing the generational-cost perspective. Meanwhile, the voltage regulation objectives are also preserved. Converter-augmented sources in a dc microgrid are grouped into two categories: dispatchable sources where their output power can be controlled, and nondispatchable sources where the output powers are set already. Examples of nondispatchable sources include renewable energy resources, where the trivial optimal solution is to set them to generate the maximum power. Such sources are considered to have their own decentralized control systems, which set their output power at the maximum level during the normal operating condition, i.e., when there is demand for their generation. Therefore, they can be modeled as a negative load demand in an economic dispatch problem. The optimization paradigm would then run on controllable sources. Similar to the classic economic dispatch problem formulation in ac systems, one can approximate the cost functions of dispatchable sources with a quadratic function [54]

$$C_i(p_i) = \alpha_i + \beta_i p_i + \gamma_i p_i^2 \tag{4}$$

where α_i, β_i, and γ_i are the coefficients of the cost functions of source i, and p_i is its output power. Then, the economic dispatch problem can be formalized as

$$\begin{aligned} \text{minimize} \quad & C(\mathbf{p}) = \sum_{i=1}^{N} C_i(p_i) \\ \text{subject to} \quad & \sum_{i=1}^{N} p_i = P_{\mathrm{demand}} - P_{\mathrm{ND}} \end{aligned} \tag{5}$$

where N is the number of dispatchable sources in the microgrid, $\mathbf{p} = [p_1 \ \dots \ p_N]^{\mathrm{T}} \in \mathbb{R}^{N\times 1}$ is the vector of output powers, P_{demand} is the total power demand of the microgrid, and P_{ND} is the generated power of nondispatchable sources. The power loss on distribution lines and the power limits of sources can also be formulated into equality and inequality constraints

$$\begin{aligned} \text{minimize} \quad & \sum_{i=1}^{N} C_i(p_i) \\ \text{subject to} \quad & \sum_{i=1}^{N} p_i = P_{\mathrm{demand}} + P_{\mathrm{loss}} - P_{\mathrm{ND}} \\ & p_{i,\min} \le p_i \le p_{i,\max} \end{aligned} \tag{6}$$

where P_{loss} is the total distribution power loss, which is a function of the voltages and network resistances. In order to solve the economic dispatch problem, the inequality constraints can be first neglected [81]. Then, the Lagrange multiplier λ and the Lagrange function [55] are defined to be minimized

$$L(\mathbf{p}, \lambda) = \sum_{i=1}^{N} C_i(p_i) + \lambda \left(P_{\mathrm{demand}} + P_{\mathrm{loss}} - P_{\mathrm{ND}} - \sum_{i=1}^{N} p_i \right). \tag{7}$$

The solution to the optimization problem is the stationary point, i.e., where all the partial derivatives of the Lagrange function L are zero [55]

$$\begin{cases} \dfrac{\partial L}{\partial p_i} = 0 \Rightarrow \dfrac{dC_i}{dp_i} = \lambda \\ \dfrac{\partial L}{\partial \lambda} = 0 \Rightarrow \sum_{i=1}^{N} p_i = P_{\mathrm{demand}} + P_{\mathrm{loss}} - P_{\mathrm{ND}}. \end{cases} \tag{8}$$

In addition to satisfying the equality constraint, the incremental costs of all the sources must be equal to λ. It should be noted that P_{demand}, P_{loss}, and P_{ND} are assumed constant (or slow varying), as common in the optimization literature [81], [82]. One can define λ_i to be the incremental cost of source i, i.e.,

$$\lambda_i = \beta_i + 2\gamma_i p_i. \tag{9}$$

Accordingly, the first equation in (8) can be written as

$$\lambda_i = \lambda \quad \forall i. \tag{10}$$

It should be noted that the consensus value, λ in (10), is not predefined, but varies with changes in the operating conditions, e.g., load change or adding/removing sources. Therefore, (10) can be written as

$$\lambda_i = \lambda_j \quad \forall i, j \tag{11}$$

which is demonstrated in Fig. 2. As an intuitive proof, one can consider a case where $\lambda_j > \lambda_k$. If the generation of source j is decreased by a small value δp, then that of source k must be increased by the same amount to satisfy the generation–consumption equality constraint. Then, the total cost change is

$$\begin{aligned} \delta C &= \sum_{i=1}^{N} \frac{dC_i}{dp_i} \delta p_i = -\lambda_j \delta p + \lambda_k \delta p \\ &= \delta p(\lambda_k - \lambda_j) < 0 \end{aligned} \tag{12}$$

which is negative. Therefore, the assumed operating point could not be the optimum. After finding the point where (8) is satisfied, the inequality constraints in (6) can be taken into account. If one or more sources operate above (below) their limits, their

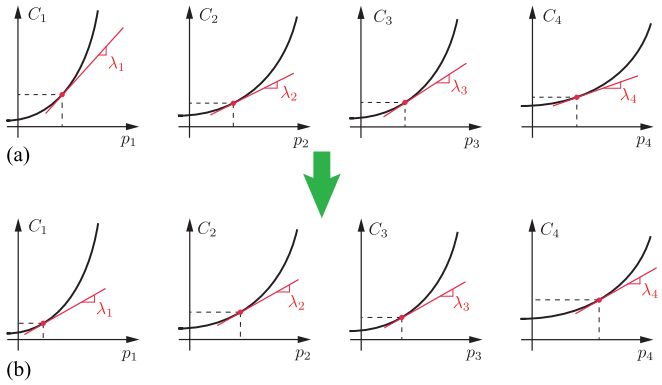

Fig. 2. Matching the incremental costs among sources in the microgrid. (a) Different incremental costs without communication among agents. (b) Identical incremental costs using communication among agents.

output power must be set at the maximum (minimum) power and excluded from (11). It should be noted that if the total demand of the microgrid is so low such that all output powers are set to the minimum, the equality constraint in (6) may not be satisfied, as nondispatchable sources are assumed to operate at their maximum power point. In that contingency, the renewable sources shall no longer operate at their maximum power, as this increases the average bus voltage of the microgrid. Accordingly, a mode transition occurs in their control systems, switching from a maximum power generation to voltage-control mode [83], [84]. Interested readers can refer to different solutions of voltage-mode control of renewable energy systems in the literature, e.g., dc bus signaling [85], [86].

IV. Unifying Optimization and Real-time Control

A. Without Generation Limits

Without loss of generality, it is first assumed that all sources are operating within their generation limits. The solution to the economic dispatch problem is the point where all incremental costs, λ_is, reach a consensus. Therefore, the controller must solve a synchronization problem among incremental costs of all sources. In order to satisfy the equality constraint, a voltage controller regulates the average of the voltages of all sources at a reference value. This reference could be either the rated voltage of the microgrid, or a set point provided by the tertiary controller. If the average voltage is regulated and the system is stable, the equality constraint is automatically met at the steady state. Otherwise, if the sum of power demand and loss is more (less) than generated power, the source voltages' would increase (decrease).

The proposed control framework for the converter i is shown in Fig. 3(a) and includes a voltage regulator and a basic optimizer, which does not consider the generation limits. The converter cooperates with neighbors on a communication graph with the adjacency matrix $\mathbf{A} = [a_{ij}] \in \mathbb{R}^{N\times N}$. The voltage controller and the optimizer generate two voltage correction terms δv_i^1 and δv_i^2, respectively. These terms are added to the microgrid's global voltage set point, $v_{\rm ref}$, to generate the voltage command for converter i, $v_{i,\rm com}$. It should be noted that $v_{\rm ref}$ is considered to be the rated voltage for all the sources. However, it can be generated by the tertiary control system of the microgrid, which can be a distributed controller [14].

The voltage regulator at converter i, shown in Fig. 3(b), estimates the average voltage of all the converters in a distributed fashion and generates a voltage correction term to regulate this estimated average on the global set point $v_{\rm ref}$ [18]. A dynamic consensus protocol is used at node i to estimate the average of all the voltages

$$\bar{v}_i = v_i + \int_0^t \sum_{j\in N_i} c a_{ij}\left(\bar{v}_j - \bar{v}_i\right) d\tau \tag{13}$$

v_i is the output voltage of converter i, $\bar{v}_i$ is the average voltage estimated by agent i, and c is the coupling gain between the voltage regulator and the optimizer. This estimated average voltage is compared with the global set point $v_{\rm ref}$ to generate an error term, which is then fed to a PI controller, $H_i(s)$, to generate the voltage correction term δv_i^1.

The proposed optimizer is shown in Fig. 3(c). It uses a local voting protocol to generate a neighborhood error term for the control agent i

$$e_i = \sum_{j\in N_i} a_{ij}\left(\lambda_j - \lambda_i\right). \tag{14}$$

The error term e_i can be written as

$$\begin{aligned} e_i &= -\lambda_i \sum_{j\in N_i} a_{ij} + \sum_{j\in N_i} a_{ij}\lambda_j \\ &= -d_i\lambda_i + \sum_{j\in N_i} a_{ij}\lambda_j \\ &= d_i\left(-\lambda_i + \sum_{j\in N_i}\frac{a_{ij}}{d_i}\lambda_j\right) \end{aligned} \tag{15}$$

i.e., the incremental cost of agent i, λ_i, is compared with a weighted average of its neighbors, $\sum a_{ij}\lambda_j/d_i$, to generate the error term e_i. This error term is then processed through a PI controller to generate a voltage correction term, δv_i^2, to regulate converter i. Therefore, if the incremental cost of source i is less (more) than the average of its neighbors, the controller increases (decreases) its voltage correction term which, in turn, increases (reduces) the voltage set point, current, power, and incremental cost of source i. Considering the same process for optimizers of all agents and proper controller design, all error terms, e_is, become zero at the steady state. This results in a consensus of λ_is, as will be shown in Section VI. Considering N agents in the graph, (15) can be also written in a matrix format as

$$\mathbf{e} = -\mathbf{D}\boldsymbol{\lambda} + \mathbf{A}\boldsymbol{\lambda} = -\mathbf{L}\boldsymbol{\lambda} \tag{16}$$

where $\mathbf{e}$ and $\boldsymbol{\lambda}$ are the vectors of all e_is and λ_is, respectively. $\mathbf{A}$, $\mathbf{D}$, and $\mathbf{L}$ are the adjacency, in-degree, and Laplacian matrices of the communication graph, respectively.

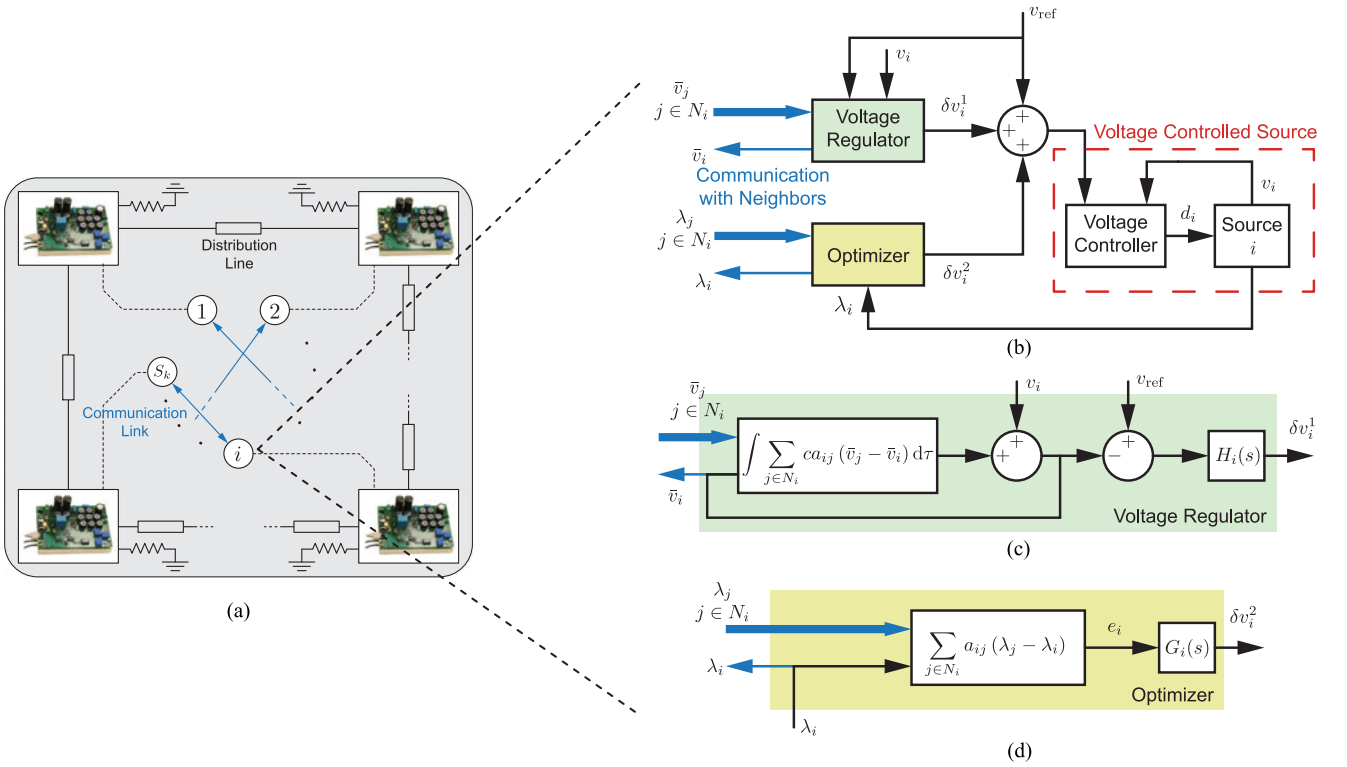

Fig. 3. Proposed distributed control structure. (a) Cyber and physical connections. (b) Controller at node i and voltage regulator at node i. (c) Basic optimizer at node i.

B. With Generation Limits

If a source reaches its maximum (minimum) generation limit, it can no longer participate in the voting protocol in (14). Instead, it keeps its generation at the maximum (minimum) level. As shown in Fig. 4(b), by modifying the proposed optimizer, instead of sharing only one variable with all the neighbors, agent i sends distinct variables to each neighbor, i.e., $\bar{\lambda}_i^j$ to agent j, which is referred to as the modified incremental cost of agent i for agent j. In addition, the communication graph is considered to be undirected, and, therefore, agent i receives $\bar{\lambda}_j^i$ from node j. As seen in Fig. 4(b), a flag is considered for each node, i.e., f_i for node i. This flag is determined by comparing the weighted average of data sent from neighbors to the minimum and maximum incremental cost of each source. Having (9), one can write the minimum and maximum incremental cost of source i as

$$\begin{cases} \lambda_{i,\max} = \beta_i + 2\gamma_i p_{i,\max} \\ \lambda_{i,\min} = \beta_i + 2\gamma_i p_{i,\min}. \end{cases} \tag{17}$$

The flag f_i determines the data to be sent to the neighbors using a logical multiplexer

$$\bar{\lambda}_i^j = \begin{cases} \lambda_i, & \mathrm{f}_i = 0 \\ \dfrac{\sum\limits_{\substack{k \in N_i \\ k \neq j}} \bar{\lambda}_k^i}{|N_i| - 1}, & \mathrm{f}_i = 1. \end{cases} \tag{18}$$

In order to describe the operation of the modified optimizer, two different scenarios are considered in Fig. 5. In Fig. 5(a), source i is considered to operate within its limits and $\mathrm{f}_i = 0$. Assuming all the neighbors of agent i to have the same operating condition, all neighbors' flags are zero, i.e., $\mathrm{f}_j = 0$ for all $j \in N_i$. Consequently

$$\bar{\lambda}_j^i = \lambda_j \qquad \forall j \in N_i. \tag{19}$$

Accordingly, the error term e_i can be written as

$$e_i = d_i \left(-\lambda_i + \sum_{j \in N_i} \frac{a_{ij}}{d_i} \bar{\lambda}_j^i \right) = d_i \left(-\lambda_i + \sum_{j \in N_i} \frac{a_{ij}}{d_i} \lambda_j \right) \tag{20}$$

which is exactly the same local voting protocol in (15). In this state, if the microgrid load is increased such that the new consensus point λ is more than $\lambda_{i,\max}$, but less than $\lambda_{j,\max}$ for all $j \in N_i$, the weighted average term in (20) becomes more than $\lambda_{i,\max}$. Consequently, as shown in Fig. 5(b), two changes occur in the control agent i: 1) the weighted average of the neighbors in (20) is bounded to $\lambda_{i,\max}$, and the error term becomes equal to

$$e_i = d_i \left(\lambda_{i,\max} - \lambda_i \right) \tag{21}$$

which regulates λ_i at $\lambda_{i,\max}$ through the controller $G_i(s)$. Accordingly, the output power of source i, p_i is regulated on $p_{i,\max}$. 2) The output of the hysteresis comparator in agent i becomes 1, which, consequently, makes f_i equal to 1. Therefore, instead of λ_i, the second term in (18) is sent to the neighbors. It should be noted that in this case, agent i sends different data to each neighbor. The data sent to neighbor j by agent i are the average

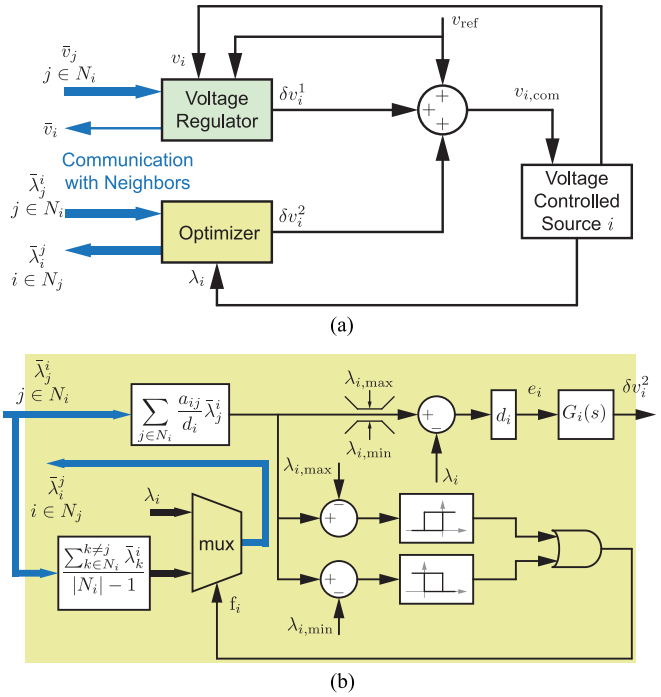

Fig. 4. Controller block diagram with modified optimizer. (a) Complete control system at node i. (b) Modified optimizer.

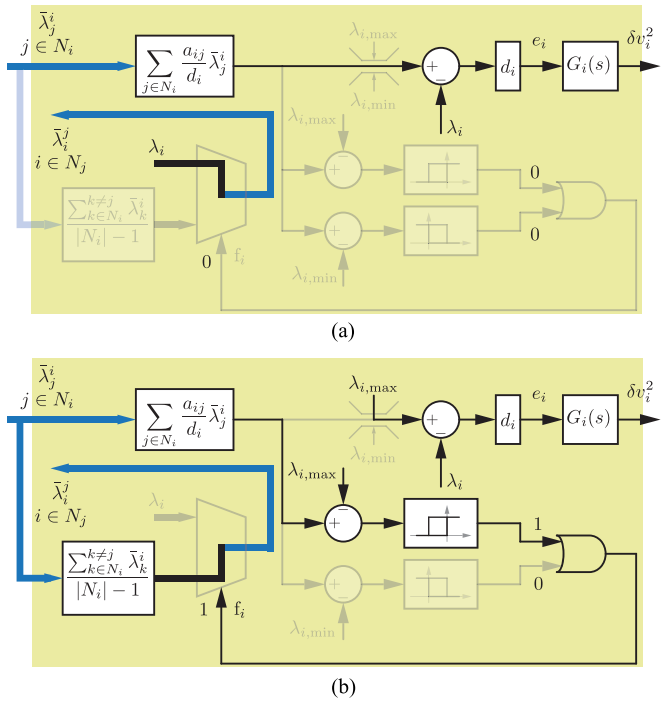

Fig. 5. Different scenarios of modified optimizer operation. (a) When P_i lies within its limits. (b) When P_i reaches its upper limit.

of the data received from all neighbors of agent i, except for agent j. Agent i plays the role of a bridge for its neighbors, i.e., neighbors of agent i remain connected and transfer data through node i. This process is explained in detail later in this section.

Once the microgrid load is decreased and the weighted average of neighbors in (20) becomes less than $\lambda_{i,\max}$ again, the output of the hysteresis comparator and f_i become zero, and the control strategy returns to the one shown in Fig. 5(a). The hysteresis comparators are used to avoid chattering. A similar change happens when a source reaches its minimum generation limit.

Agent changes its control strategy upon reaching its generation limit, the operation of other agents can be considered as a cooperative control with the basic strategy shown in Fig. 3(c) and a modified adjacency matrix, whose dimension is one less than the original adjacency matrix. This is demonstrated in Fig. 6, where agent 3 reaches its generation limit. The communication graph is considered to be undirected and all nonzero communication weights are assumed equal. As seen in Fig. 6(a), when all the sources are operating within their limits, each agent sends its incremental cost to its neighbors. The adjacency matrix is symmetric, and therefore, the corresponding Laplacian matrix is balanced. Assuming that one of the sources, e.g., Source 3, has reached its maximum/minimum generation limit, its agent send different data to its three neighbors, i.e., average incremental costs of every two neighbors to the third neighbor. Accordingly, the communication among agents can be shown, as in Fig. 6(b), which has a corresponding adjacency matrix, with the entries of the third column and the third row all equal to zero. As node 3 acts only as a bridge among its neighbors, the new data exchange pattern among the nodes can be represented with a modified graph with one node less than the original graph. Fig. 6(b) shows this modified communication graph, where node 3 is eliminated, and its corresponding adjacency matrix $\mathbf{A}'$, which is still symmetric with a balanced Laplacian matrix.

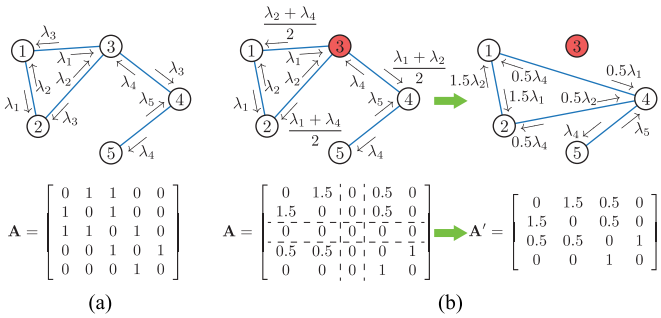

Fig. 6. Changes in information exchange in optimizer upon reaching a source to its generation limit.

V. Dynamic Model Development

A system-level dynamic model, consisting of the proposed controller/optimizer, communication network, and the physical microgrid (power converters and power distribution network), is developed. Using the resulting model, one can see if the control objectives, i.e., voltage regulation and minimization of total generational costs, are achieved.

A. Dynamic Model of the Distributed Controller

A more general case where one source has reached its maximum generation limit is considered, e.g., source N. Therefore, as shown in Section IV-B, the cooperation among the first $N-1$ agents can be considered as a local voting protocol given in (14) with a modified adjacency matrix, whose corresponding balanced Laplacian matrix is represented by $\mathbf{L}' \in \mathbb{R}^{(N-1)\times(N-1)}$. This general case can easily be modified for the case where no sources, or more than one source, have reached their generational limits. Similar to (16), (14) for $N-1$ sources can be written in the matrix format as

$$\mathbf{e}_{N-1} = -\mathbf{L}'\boldsymbol{\lambda}_{N-1} \tag{22}$$

where $\mathbf{e}_{N-1} = [e_1 \ \ldots \ e_{N-1}]^{\mathrm{T}}$ and $\boldsymbol{\lambda}_{N-1} = [\lambda_1 \ \ldots \ \lambda_{N-1}]^{\mathrm{T}} \in \mathbb{R}^{(N-1)\times 1}$ are the vectors of errors and incremental costs for the first $N-1$ agents, respectively. Using (21), the corresponding error term for source N, that has reached its maximum generation limit, can be written as

$$e_N = d_N\left(\lambda_{N,\max} - \lambda_N\right). \tag{23}$$

As (22) is a set of $N-1$ scalar equations and (23) is a single scalar equation, the combination of two equations can be written as a set of N equations in a matrix format

$$\mathbf{e} = -\left(\mathbf{L}''\boldsymbol{\lambda} + \mathbf{D}_N\left(\boldsymbol{\lambda} - \boldsymbol{\lambda}_{\max}\right)\right) \tag{24}$$

where $\mathbf{e} = [e_1 \ \ldots \ e_N]^{\mathrm{T}}$, $\boldsymbol{\lambda} = [\lambda_1 \ \ldots \ \lambda_N]^{\mathrm{T}}$, and $\boldsymbol{\lambda}_{\max} = \left[\lambda_{1,\max} \ \ldots \ \lambda_{N,\max}\right]^{\mathrm{T}} \in \mathbb{R}^{N\times 1}$ are the global vectors of errors, incremental costs, and maximum incremental costs, respectively. $\mathbf{D}_N$ is an $N \times N$ matrix, whose (N,N) entry is d_N and other entries are zero. $\mathbf{L}''$ is defined as

$$\mathbf{L}'' = \left[\begin{array}{ccc|c} & & & 0 \\ & \mathbf{L}' & & \vdots \\ & & & 0 \\ \hline 0 & \ldots & 0 & 0 \end{array}\right]. \tag{25}$$

One can write (24) as

$$\begin{aligned}\mathbf{e} &= -\left(\mathbf{L}'' + \mathbf{D}_N\right)\boldsymbol{\lambda} + \mathbf{D}_N\boldsymbol{\lambda}_{\max} \\ &= -\mathbf{L}^{+}\boldsymbol{\lambda} + \mathbf{D}_N\boldsymbol{\lambda}_{\max}\end{aligned} \tag{26}$$

where $\mathbf{L}^{+}$ is defined as

$$\mathbf{L}^{+} = \left[\begin{array}{ccc|c} & & & 0 \\ & \mathbf{L}' & & \vdots \\ & & & 0 \\ \hline 0 & \ldots & 0 & d_N \end{array}\right]. \tag{27}$$

Then, one can write (26) in the frequency domain

$$\mathbf{E} = -\mathbf{L}^{+}\boldsymbol{\Lambda} + \mathbf{D}_N\boldsymbol{\Lambda}_{\max} \tag{28}$$

where $\mathbf{E}$, $\boldsymbol{\Lambda}$, and $\boldsymbol{\Lambda}_{\max} = \boldsymbol{\lambda}_{\max}s^{-1}$ are the Laplace transforms of $\mathbf{e}$, $\boldsymbol{\lambda}$, and $\boldsymbol{\lambda}_{\max}$, respectively.

Similarly, (10) can be written as

$$\boldsymbol{\lambda} = \boldsymbol{\beta} + 2\boldsymbol{\Gamma}\mathbf{p} \tag{29}$$

where $\boldsymbol{\beta} = \left[\beta_1 \ \ldots \ \beta_N\right]^{\mathrm{T}} \in \mathbb{R}^{N\times 1}$ and $\boldsymbol{\Gamma} = \mathrm{diag}\{\gamma_i\} \in \mathbb{R}^{N\times N}$. In the frequency domain

$$\boldsymbol{\Lambda} = \mathbf{B} + 2\boldsymbol{\Gamma}\mathbf{P} \tag{30}$$

where $\mathbf{P}$ and $\mathbf{B} = \boldsymbol{\beta}s^{-1}$ are the Laplace transforms of $\mathbf{p}$ and $\boldsymbol{\beta}$, respectively. Using (28) and (30), the optimizer output can be written as

$$\begin{aligned}\Delta\mathbf{V}^2 &= -\mathbf{G}\mathbf{L}^{+}\boldsymbol{\Lambda} + \mathbf{G}\mathbf{D}_N\boldsymbol{\Lambda}_{\max} \\ &= -\mathbf{G}\mathbf{L}^{+}\left(\mathbf{B} + 2\boldsymbol{\Gamma}\mathbf{P}\right) + \mathbf{G}\mathbf{D}_N\boldsymbol{\Lambda}_{\max}\end{aligned} \tag{31}$$

where $\Delta\mathbf{V}^2$ is the Laplace transform of $\delta\mathbf{v}^2 = [\delta v_1^2 \ \ldots \ \delta v_N^2]^{\mathrm{T}} \in \mathbb{R}^{N\times 1}$ and $\mathbf{G} = \mathrm{diag}\{G_i(s)\} \in \mathbb{R}^{N\times N}$ is the PI-controller matrix of the optimizer.

On the other hand, as shown in [18], the average voltage estimation in (13) can be written as

$$\bar{\mathbf{V}} = s\left(s\mathbf{I}_N + c\mathbf{L}\right)^{-1}\mathbf{V} = \mathbf{H}_{\mathrm{est}}\mathbf{V} \tag{32}$$

where $\bar{\mathbf{V}}$ and $\mathbf{V}$ are the Laplace transforms of $\bar{\mathbf{v}} = [\bar{v}_1 \ \ldots \ \bar{v}_N]^{\mathrm{T}}$ and $\mathbf{v} = [v_1 \ \ldots \ v_N]^{\mathrm{T}} \in \mathbb{R}^{N\times 1}$, respectively. $\mathbf{I}_N$ and $\mathbf{H}_{\mathrm{est}} \in \mathbb{R}^{N\times N}$ are the identity matrix and the estimator transfer function, respectively. It is shown in [18] that if $\mathbf{L}$ is balanced, then all elements of $\bar{\mathbf{v}}$ converge to the average of elements of $\mathbf{v}$ at the steady state. Then, the voltage controller can be written as

$$\Delta\mathbf{V}^1 = \mathbf{H}\left(\mathbf{V}_{\mathrm{ref}} - \bar{\mathbf{V}}\right) = \mathbf{H}\left(\mathbf{V}_{\mathrm{ref}} - \mathbf{H}_{\mathrm{est}}\mathbf{V}\right) \tag{33}$$

where $\Delta\mathbf{V}^1$ are $\mathbf{V}_{\mathrm{ref}}$ are the Laplace transforms of $\delta\mathbf{v}^1 = \left[\delta v_1^1 \ \ldots \ \delta v_N^1\right]^{\mathrm{T}}$ and $\mathbf{v}_{\mathrm{ref}} = \left[v_{\mathrm{ref}} \ \ldots \ v_{\mathrm{ref}}\right]^{\mathrm{T}} \in \mathbb{R}^{N\times 1}$, respectively, and $\mathbf{H} = \mathrm{diag}\{H_i(s)\} \in \mathbb{R}^{N\times N}$. Then, the commanded source voltages can be written as

$$\begin{aligned}\mathbf{V}_{\mathrm{com}} &= \mathbf{V}_{\mathrm{ref}} + \Delta\mathbf{V}^1 + \Delta\mathbf{V}^2 \\ &= \mathbf{V}_{\mathrm{ref}} + \mathbf{H}\left(\mathbf{V}_{\mathrm{ref}} - \mathbf{H}_{\mathrm{est}}\mathbf{V}\right) \\ &\quad - \mathbf{G}\mathbf{L}^{+}\left(\mathbf{B} + 2\boldsymbol{\Gamma}\mathbf{P}\right) + \mathbf{G}\mathbf{D}_N\boldsymbol{\Lambda}_{\max}\end{aligned} \tag{34}$$

where $\mathbf{V}_{\mathrm{com}}$ is the Laplace transform of $\mathbf{v}_{\mathrm{com}} = [v_{1,\mathrm{com}} \ \ldots \ v_{N,\mathrm{com}}]^{\mathrm{T}} \in \mathbb{R}^{N\times 1}$. Equation (34) expresses the controller output $\mathbf{V}_{\mathrm{com}}$ in terms of its inputs, $\mathbf{V}_{\mathrm{ref}}$, $\mathbf{V}$, and $\mathbf{P}$, and concludes the controller modeling.

B. Combined Microgrid and Controller Models

The overall system model can be obtained by combining the controller and microgrid transfer functions. The input of the microgrid transfer function is $\mathbf{V}_{\mathrm{com}}$ and its outputs are $\mathbf{V}$ and $\mathbf{P}$. Then, the system-level transfer functions, which are from the system input, $\mathbf{V}_{\mathrm{ref}}$, to the desired outputs, i.e., $\boldsymbol{\Lambda}$ and $\mathbf{V}$, can be found. The voltage-controlled converters in microgrids can be represented as

$$V_i = G_{i,\mathrm{cl}}(s)V_{i,\mathrm{com}} \tag{35}$$

where $G_{i,\mathrm{cl}}(s)$ is the closed-loop transfer function of the converter i. V_i and $V_{i,\mathrm{ref}}$ are the Laplace transforms of v_i and $v_{i,\mathrm{ref}}$, respectively. Considering all converters, (35) can be written in a matrix format as

$$\mathbf{V} = \mathbf{G}_{\mathrm{cl}}\mathbf{V}_{\mathrm{com}}. \tag{36}$$

The admittance matrix of the microgrid, $\mathbf{Y}$, carries the parameters of the distribution grid, and its entries are defined as

$$y_{ij} = \begin{cases} -\dfrac{1}{z_{ij}}, & i \neq j \\ \sum\limits_{k} \dfrac{1}{z_{ik}}, & i = j \end{cases} \tag{37}$$

where z_{ij} and z_{ii} are the impedance between bus i and bus j and between bus i and ground, respectively. It should be noted that the output node of each source is considered as a bus in the microgrid, and the number of buses is equal to the number of sources. The source currents can be written as

$$\mathbf{I} = \mathbf{YV} = \mathbf{YG}_{\rm cl}\mathbf{V}_{\rm com}. \tag{38}$$

Once the transfer functions from $\mathbf{V}_{\rm com}$ to $\mathbf{V}$ and $\mathbf{I}$ are found, the transfer function from $\mathbf{V}_{\rm com}$ to $\mathbf{P}$ must be found to complete the system-level modeling using (34). Since each source output is the product of its voltage and current, the transfer function from $\mathbf{V}_{\rm com}$ to the vector of output powers $\mathbf{P}$ cannot be found directly. Instead, using small-signal modeling, the perturbation of source power i, $\tilde{p}_i$, can be written as

$$\tilde{p}_i = \bar{V}_i\tilde{i}_i + \tilde{v}_i\bar{I}_i \tag{39}$$

where $\bar{V}_i$ and $\bar{I}_i$ are the output voltage and current of source i at the operating point, respectively, and $\tilde{v}_i$ and $\tilde{i}_i$ are their perturbations, respectively. Since the current perturbation is much larger than that of the voltage, (39) can be written as

$$\tilde{p}_i \simeq \bar{V}_i\tilde{i}_i. \tag{40}$$

The output voltage of source i at the operating point is the rated voltage of the microgrid, $V_{\rm rated}$. Then, (40) can be written as

$$\tilde{p}_i = V_{\rm rated}\tilde{i}_i \quad \forall i. \tag{41}$$

Accordingly, (34) can be written as

$$\begin{aligned} \mathbf{V}_{\rm com} = \ & \mathbf{V}_{\rm ref} + \mathbf{H}\left(\mathbf{V}_{\rm ref} - \mathbf{H}_{\rm est}\mathbf{V}\right) \\ & - \mathbf{GL}^{+}\left(\mathbf{B} + 2V_{\rm rated}\mathbf{\Gamma I}\right) + \mathbf{GD}_N\mathbf{\Lambda}_{\max}. \end{aligned} \tag{42}$$

One can define $\mathbf{C} \triangleq 2V_{\rm rated}\mathbf{\Gamma}$ and write (42) as

$$\begin{aligned} \mathbf{V}_{\rm com} = \ & \mathbf{V}_{\rm ref} + \mathbf{H}\left(\mathbf{V}_{\rm ref} - \mathbf{H}_{\rm est}\mathbf{V}\right) \\ & - \mathbf{GL}^{+}\left(\mathbf{B} + \mathbf{CI}\right) + \mathbf{GD}_N\mathbf{\Lambda}_{\max}. \end{aligned} \tag{43}$$

Substituting $\mathbf{V}_{\rm com}$ and $\mathbf{I}$ from (36) and (38), one can write (43) as

$$\begin{aligned} \mathbf{G}_{\rm cl}^{-1}\mathbf{V} = \ & \mathbf{V}_{\rm ref} + \mathbf{H}\left(\mathbf{V}_{\rm ref} - \mathbf{H}_{\rm est}\mathbf{V}\right) \\ & - \mathbf{GL}^{+}\left(\mathbf{B} + \mathbf{CYV}\right) + \mathbf{GD}_N\mathbf{\Lambda}_{\max}. \end{aligned} \tag{44}$$

Using (44), the vector of output voltages $\mathbf{V}$ can be expressed as

$$\begin{aligned} \mathbf{V} = \ & \left(\mathbf{G}_{\rm cl}^{-1} + \mathbf{HH}_{\rm est} + \mathbf{GL}^{+}\mathbf{CY}\right)^{-1} \\ & \times \left(\left(\mathbf{I}_N + \mathbf{H}\right)\mathbf{V}_{\rm ref} - \mathbf{GL}^{+}\mathbf{B} + \mathbf{GD}_N\mathbf{\Lambda}_{\max}\right) \end{aligned} \tag{45}$$

where $\mathbf{I}_N \in \mathbb{R}^{N\times N}$ is the identity matrix. Accordingly, the vector of incremental costs $\mathbf{\Lambda}$ can be written as

$$\begin{aligned} \mathbf{\Lambda} = \ & \mathbf{B}s^{-1} + \mathbf{CY}\left(\mathbf{G}_{\rm cl}^{-1} + \mathbf{HH}_{\rm est} + \mathbf{GL}^{+}\mathbf{CY}\right)^{-1} \\ & \times \left(\left(\mathbf{I}_N + \mathbf{H}\right)\mathbf{V}_{\rm ref} - \mathbf{GL}^{+}\mathbf{B} + \mathbf{GD}_N\mathbf{\Lambda}_{\max}\right). \end{aligned} \tag{46}$$

Due to the presence of the terms $\mathbf{B}$ and $\mathbf{\Lambda}_{\max}$, (45) and (46) are not in the form of transfer functions from $\mathbf{V}_{\rm ref}$ to $\mathbf{V}$ and $\mathbf{\Lambda}$. However, $\mathbf{B}$ and $\mathbf{\Lambda}_{\max}$ may be considered as step inputs to the system and the transfer functions of the system with three inputs, $\mathbf{V}_{\rm ref}$, $\mathbf{B}$, and $\mathbf{\Lambda}_{\max}$, can be found. One can express (45) and (46) as

$$\begin{cases} \mathbf{V} = \mathbf{T}_{vv}\mathbf{V}_{\rm ref} + \mathbf{T}_{v\beta}\mathbf{B} + \mathbf{T}_{v\lambda}\mathbf{\Lambda}_{\max} \\ \mathbf{\Lambda} = \mathbf{T}_{\lambda v}\mathbf{V}_{\rm ref} + \mathbf{T}_{\lambda\beta}\mathbf{B} + \mathbf{T}_{\lambda\lambda}\mathbf{\Lambda}_{\max} \end{cases} \tag{47}$$

where the six transfer functions in (47) are given by

$$\begin{cases} \mathbf{T}_{vv} = \left(\mathbf{G}_{\rm cl}^{-1} + \mathbf{HH}_{\rm est} + \mathbf{GL}^{+}\mathbf{CY}\right)^{-1}\left(\mathbf{I}_N + \mathbf{H}\right) \\ \mathbf{T}_{v\beta} = -\left(\mathbf{G}_{\rm cl}^{-1} + \mathbf{HH}_{\rm est} + \mathbf{GL}^{+}\mathbf{CY}\right)^{-1}\mathbf{GL}^{+} \\ \mathbf{T}_{v\lambda} = \left(\mathbf{G}_{\rm cl}^{-1} + \mathbf{HH}_{\rm est} + \mathbf{GL}^{+}\mathbf{CY}\right)^{-1}\mathbf{GD}_N \\ \mathbf{T}_{\lambda v} = \mathbf{CYT}_{vv} \\ \mathbf{T}_{\lambda\beta} = \mathbf{I}_N + \mathbf{CYT}_{v\beta} \\ \mathbf{T}_{\lambda\lambda} = \mathbf{CYT}_{v\lambda}. \end{cases} \tag{48}$$

It is noteworthy that when no source has reached its generation limits, the transfer functions can be found by setting $\mathbf{L}^{+}$ and $\mathbf{D}_N$ to $\mathbf{L}$ and $\mathbf{0}$, respectively.

C. Design Guidelines

Without loss of generality, one can set the controller parameters considering that no source has reached its generation limits. Considering the transfer functions in (48), the design parameters are the weights of communication links (equivalently Laplacian matrix $\mathbf{L}$), coupling gain c (equivalently estimator transfer function $\mathbf{H}_{\rm est}$), and controller transfer function matrices, $\mathbf{H}$ and $\mathbf{G}$. After setting the Laplacian matrix $\mathbf{L}$ and the coupling gain c, one can design the voltage regulator and optimizer controller matrices, $\mathbf{H}$ and $\mathbf{G}$, to provide any desired asymptotically stable dynamic response, where all the poles of (48) lie in the open left hand plane (OLHP). More studies are performed in Section VII on a microgrid prototype to demonstrate the controller design process.

VI. Steady-State Analysis

The steady-state performance of the proposed controller must be analyzed to validate the fulfillment of the control objectives, i.e., voltage regulation and cost minimization. The voltage set point $v_{i,\rm ref}$ is considered to be the same for all agents ($v_{i,\rm ref} = v_{\rm ref}, \forall i$). Accordingly, $\mathbf{V}_{\rm ref}$ can be written as

$$\mathbf{V}_{\rm ref} = \underline{\mathbf{1}}v_{\rm ref}s^{-1}. \tag{49}$$

One can assume stability of the output voltages. Accordingly, $\mathbf{V}$ is a type 1 vector (has one pole at the origin and some other poles in the OLHP). Therefore, the final value theorem can be used to find the steady-state value of the output voltages

vector, $\mathbf{v}^{\rm ss}$,

$$\begin{aligned}\mathbf{v}^{\rm ss} &= \lim_{s\to 0} s\mathbf{V}\\ &= \lim_{s\to 0}\left(s\mathbf{G}_{\rm cl}^{-1}+s\mathbf{H}\mathbf{H}_{\rm est}+s\mathbf{G}\mathbf{L}^{+}\mathbf{C}\mathbf{Y}\right)^{-1}\\ &\quad\times\left(s\left(\mathbf{I}_N+\mathbf{H}\right)\underline{1}v_{\rm ref}-s\mathbf{G}\mathbf{L}^{+}\boldsymbol{\beta}+s\mathbf{G}\mathbf{D}_N\boldsymbol{\lambda}_{\max}\right).\end{aligned}\tag{50}$$

Since the controller matrices $\mathbf{G}$ and $\mathbf{H}$ are diagonal PI matrices, they can be written as $\mathbf{G}=\mathbf{G}_{\rm P}+\mathbf{G}_{\rm I}s^{-1}$ and $\mathbf{H}=\mathbf{H}_{\rm P}+\mathbf{H}_{\rm I}s^{-1}$, where $\mathbf{G}_{\rm P}$, $\mathbf{G}_{\rm I}$, $\mathbf{H}_{\rm P}$, and $\mathbf{H}_{\rm I}$ are constant diagonal matrices carrying the proportional and integral gains of the controllers $G_i(s)$ and $H_i(s)$ for all the agents. In addition, the dc gain of the closed-loop transfer functions $G_{i,{\rm cl}}(s)$ in (35) is one, i.e, $\mathbf{G}_{\rm cl}=\mathbf{I}_N$. In addition, as shown in [18], $\lim_{s\to 0}\mathbf{H}_{\rm est}=\mathbf{Q}_N$, where $\mathbf{Q}_N\in\mathbb{R}^{N\times N}$ is the averaging matrix, whose entries are all $1/N$. Therefore, (50) can be written as

$$\begin{aligned}\mathbf{v}^{\rm ss} &= \left(\mathbf{H}_{\rm I}\mathbf{Q}_N+\mathbf{G}_{\rm I}\mathbf{L}^{+}\mathbf{C}\mathbf{Y}_{\rm dc}\right)^{-1}\\ &\quad\times\left(\mathbf{H}_{\rm I}\underline{1}v_{\rm ref}-\mathbf{G}_{\rm I}\mathbf{L}^{+}\boldsymbol{\beta}+\mathbf{G}_{\rm I}\mathbf{D}_N\boldsymbol{\lambda}_{\max}\right)\end{aligned}\tag{51}$$

where $\mathbf{Y}_{\rm dc}$ is the dc admittance matrix of the microgrid, where all the inductors are shorted and all the capacitors are opened. Defining the diagonal matrix $\mathbf{R}_{\rm I}=\mathbf{G}_{\rm I}^{-1}\mathbf{H}_{\rm I}$, one can express (51) as

$$\left(\mathbf{R}_{\rm I}\mathbf{Q}_N+\mathbf{L}^{+}\mathbf{C}\mathbf{Y}_{\rm dc}\right)\mathbf{v}^{\rm ss}=\mathbf{R}_{\rm I}\underline{1}v_{\rm ref}-\mathbf{L}^{+}\boldsymbol{\beta}+\mathbf{D}_N\boldsymbol{\lambda}_{\max}.\tag{52}$$

Then, one can define a modified averaging matrix as

$$\mathbf{Q}'_N=\left[\begin{array}{ccc|c}&&&0\\&\mathbf{Q}_{N-1}&&\vdots\\&&&0\\\hline 0&\cdots&0&0\end{array}\right]\tag{53}$$

where $\mathbf{Q}_{N-1}$ is the $(N-1)\times(N-1)$ averaging matrix. Given $\mathbf{Q}'_N$, $\mathbf{D}_N$, and $\mathbf{L}^{+}$, and since $\mathbf{L}'$ is balanced, one can conclude that $\mathbf{Q}'_N\mathbf{L}^{+}=\mathbf{0}$ and $\mathbf{Q}'_N\mathbf{D}_N=\mathbf{0}$. Therefore, by multiplying $\mathbf{Q}'_N$ from the left in the both sides of (52), one can write

$$\mathbf{Q}'_N\mathbf{R}_{\rm I}\mathbf{Q}_N\mathbf{v}^{\rm ss}=\mathbf{Q}'_N\mathbf{R}_{\rm I}\underline{1}v_{\rm ref}.\tag{54}$$

In addition, according to definition of the averaging matrix, $\mathbf{Q}_N\mathbf{v}^{\rm ss}=\underline{1}\left\langle\mathbf{v}^{\rm ss}\right\rangle$, where the scalar $\left\langle\mathbf{v}^{\rm ss}\right\rangle$ is the average of the elements of $\mathbf{v}^{\rm ss}$, i.e., the average of the output voltages at the steady state. Accordingly, (54) can be written as

$$\mathbf{Q}'_N\mathbf{R}_{\rm I}\underline{1}\left\langle\mathbf{v}^{\rm ss}\right\rangle=\mathbf{Q}'_N\mathbf{R}_{\rm I}\underline{1}v_{\rm ref}.\tag{55}$$

Since $\mathbf{Q}'_N\mathbf{R}_{\rm I}\underline{1}$ is a nonzero vector, one can conclude that $\left\langle\mathbf{v}^{\rm ss}\right\rangle=v_{\rm ref}$, i.e., the average of the output voltages is equal to the global voltage set point of the microgrid.

On the other hand, (52) can be expressed as

$$\mathbf{R}_{\rm I}\underline{1}\left\langle\mathbf{v}^{\rm ss}\right\rangle+\mathbf{L}^{+}\left(\boldsymbol{\beta}+\mathbf{C}\mathbf{Y}_{\rm dc}\mathbf{v}^{\rm ss}\right)=\mathbf{R}_{\rm I}\underline{1}v_{\rm ref}+\mathbf{D}_N\boldsymbol{\lambda}_{\max}\tag{56}$$

or, equivalently

$$\mathbf{L}^{+}\boldsymbol{\lambda}^{\rm ss}=\mathbf{D}_N\boldsymbol{\lambda}_{\max}.\tag{57}$$

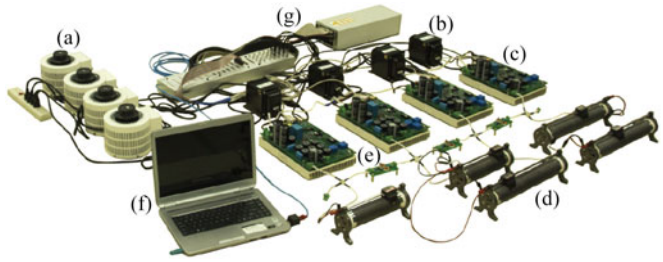

Fig. 7. Experimental setup of a dc microgrid. (a) Autotransformers. (b) Isolation transformers. (c) Rectifiers followed by dc–dc buck converters. (d) Resistive loads. (e) Distribution lines. (f) Programming and monitoring computer. (g) dSPACE DS1103 control boards.

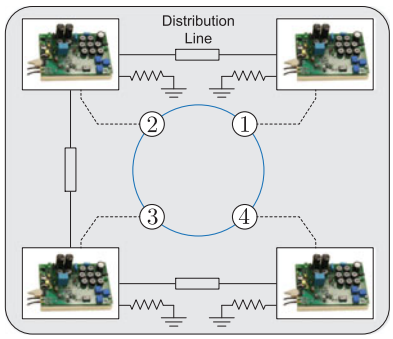

Fig. 8. Electrical and cyber connections of the prototyped dc microgrid.

Substituting $\mathbf{L}^{+}$ from (27), one can write (52) as

$$\begin{cases}\mathbf{L}'\boldsymbol{\lambda}^{\rm ss}_{N-1}=\mathbf{0}\\ \lambda^{\rm ss}_N=\lambda_{N,\max}.\end{cases}\tag{58}$$

Since the modified Laplacian matrix $\mathbf{L}'$ has a spanning tree, the first expression in (58) results in the same values for $\lambda^{\rm ss}_1$ to $\lambda^{\rm ss}_{N-1}$. Therefore, the incremental costs are balanced at the steady state for sources that have not reached their limits. For a source N that has reached its limit, the incremental cost (output power) is regulated at its maximum value.

VII. Experimental Verification

A dc microgrid setup, including four energy sources and four resistive loads as shown in Fig. 7, is prototyped to study the performance of the proposed controller. Each energy source is implemented using an isolation transformer, an autotransformer, and an ac–dc buck converter. The isolation transformers are used to provide galvanic isolation, while the autotransformers are used to adjust the input voltage of the converters. A dSPACE DS1103 control platform is used to implement the proposed control routines. Fig. 8 shows the schematic of electrical connections of the microgrid and the sparse communication network spanned among the sources. The distribution lines among the sources are represented with π-models. The electrical specifications of the prototyped microgrid are tabulated in the Appendix. The buck converters' parameters and the cost-function coefficients of each source are also provided in the Appendix. The communication links are all bidirectional. The communication weights are $a_{ij}=a_{ji}=1.25$ for any pair of connected agents (i,j). Other control parameters can also be found in the

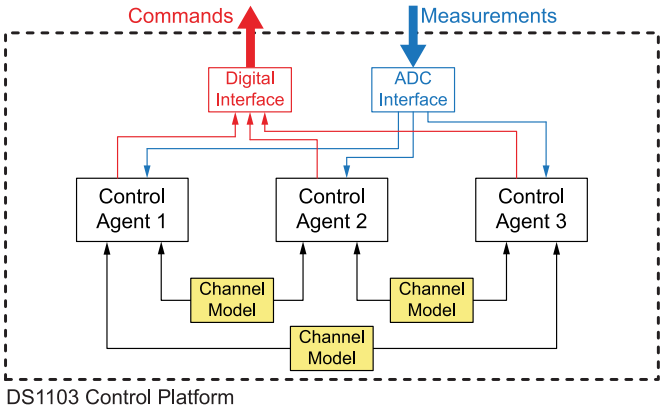

Fig. 9. Block diagram of the control system inside DS1103 platform.

Appendix. It should be noted that the proposed distributed control method is replicated in detail with separate modules on a dSPACE control platform. The modular implementation of the distributed system is shown in Fig. 9, where the control agents and communication channel models are implemented in a fully distributed fashion. Using this method of implementation, the single dSPACE controller behaves as if there are a group of physically separated controllers cooperating through communication links to handle the control objectives. Each module has its own enable/disable control input, which allows us to replicate the failure in different parts of the system. Using this setup, the frequency-domain characteristics are studied. In addition, the prototyped microgrid is simulated in MATLAB/Simulink using PLECS blocksets. Then, the proposed controller performance is verified through different cases studies, including simulation and experimental, in two categories, i.e., normal operating condition and faults.

A. *Frequency-Domain Characteristics*

To design the control parameters, the frequency response of the transfer functions in (48) can be studied. For brevity, the voltage transfer functions $\mathbf{T}_{vv}$ and $\mathbf{T}_{v\beta}$ are studied. Without loss of generality, it is assumed that none of the sources have reached their limits. Since all elements of $\mathbf{V}_{\rm ref}$ are considered to be the same, one can write

$$\mathbf{T}_{vv}\mathbf{V}_{\rm ref} = \mathbf{T}_{vv}\underline{\mathbf{1}}V_{\rm ref} = \underline{\mathbf{T}}_{vv}V_{\rm ref} \tag{59}$$

where element i of $\underline{\mathbf{T}}_{vv}$ is the sum of elements on the ith row of $\mathbf{T}_{vv}$. For a system of four sources, $\underline{\mathbf{T}}_{vv}$ is a 4-by-1 matrix. The Bode diagrams of the four elements of this matrix are shown in Fig. 10. The closed-loop transfer functions of individual converters $G_{i,\rm cl}$ are first extracted experimentally; then, the transfer functions are obtained using (48) and (59). As shown, all voltage transfer functions exhibit a similar response to the change of voltage set point. The transfer function $\mathbf{T}_{v\beta}$ is a 4-by-4 matrix and the Bode diagrams of the four elements of its first column are presented in Fig. 11, which are transfer functions from the incremental cost coefficient B_1 to all output voltages. As seen, at low frequencies, the output voltage V_1 has the largest response to the perturbation of B_1 compared to other three voltages. V_2

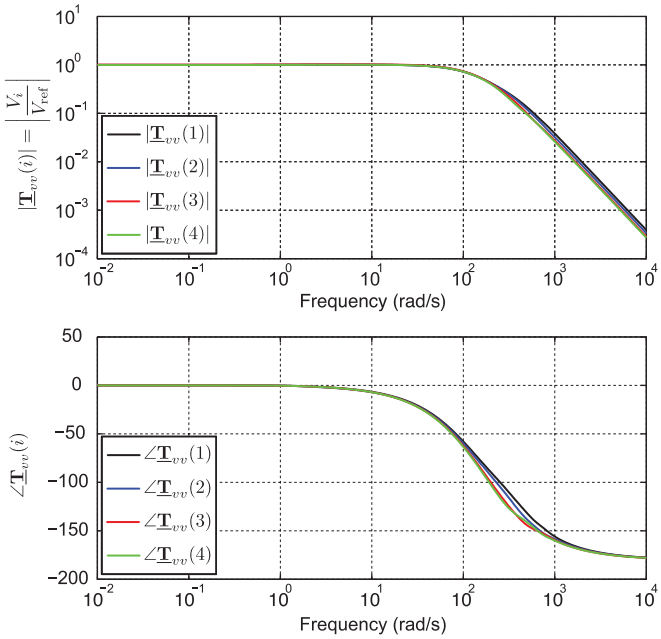

Fig. 10. Transfer functions from the voltage set point $V_{\rm ref}$ to output voltages V_i.

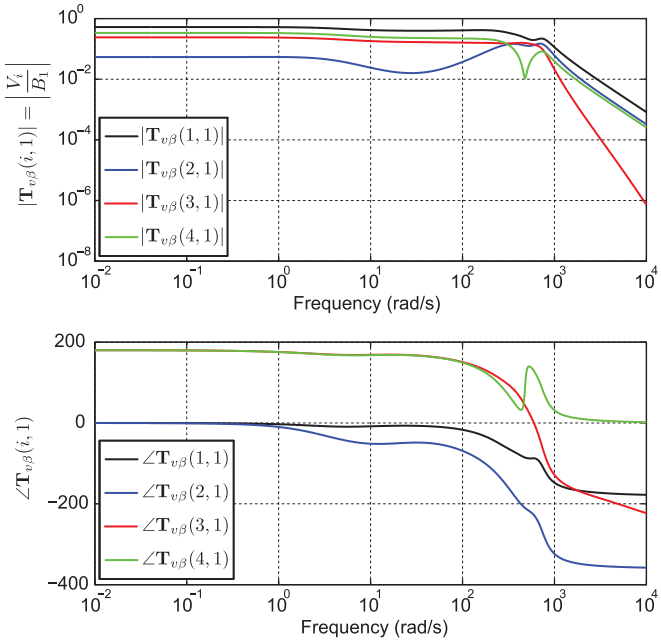

Fig. 11. Transfer functions from cost coefficient B_1 to output voltages V_i.

have a small amplitude response, but V_3 and V_4 has inverse responses (-180° phase). It should be noted that since $V_{\rm ref}$ is not changed and the controller maintains the average (sum) of voltages constant, the sum of four responses at low frequencies (steady-state) must be zero, which can be seen in Fig. 11.

Next, the poles of the first element of $\underline{\mathbf{T}}_{vv}$ are found using an estimation of the transfer function in (48). It should be noted that since the original transfer function has a high order, a second-order estimation is obtained for this study. The movement of the two poles of the system is shown in Fig. 12 as the nonzero

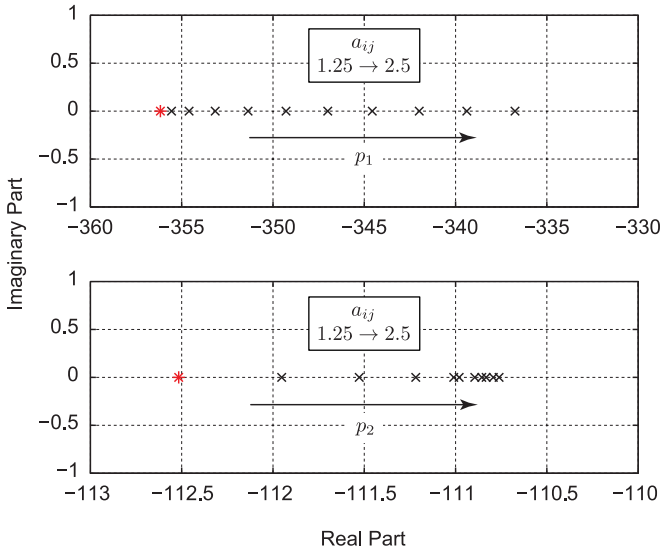

Fig. 12. Pole movements, for the transfer function from V_{ref} to V_1, as communication weight change.

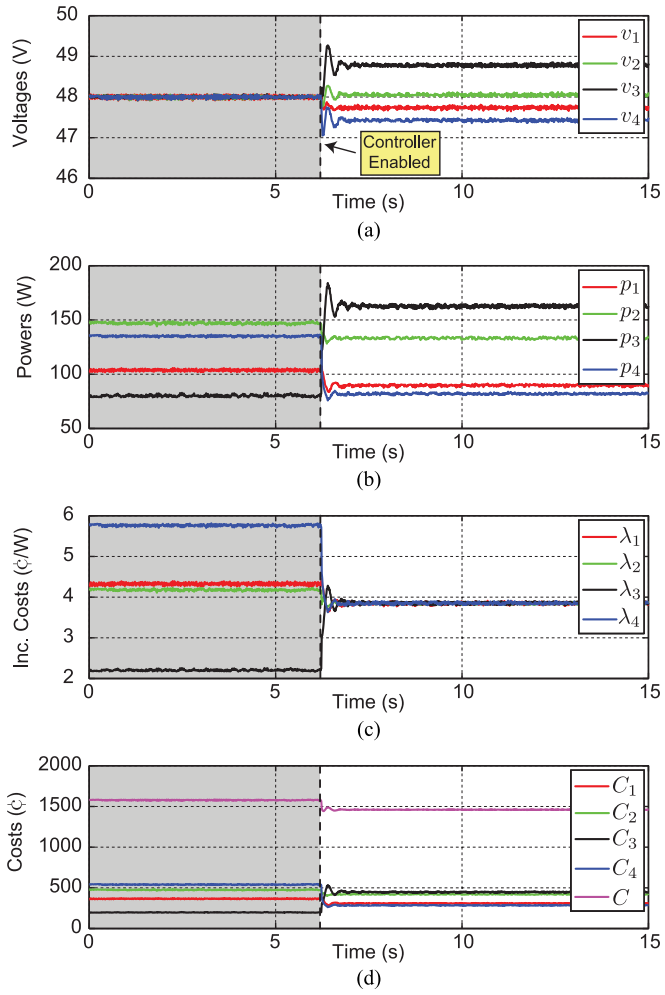

Fig. 13. Controller performance in cost minimization and voltage regulation. (a) Voltages. (b) Powers. (c) Incremental costs. (d) Costs.

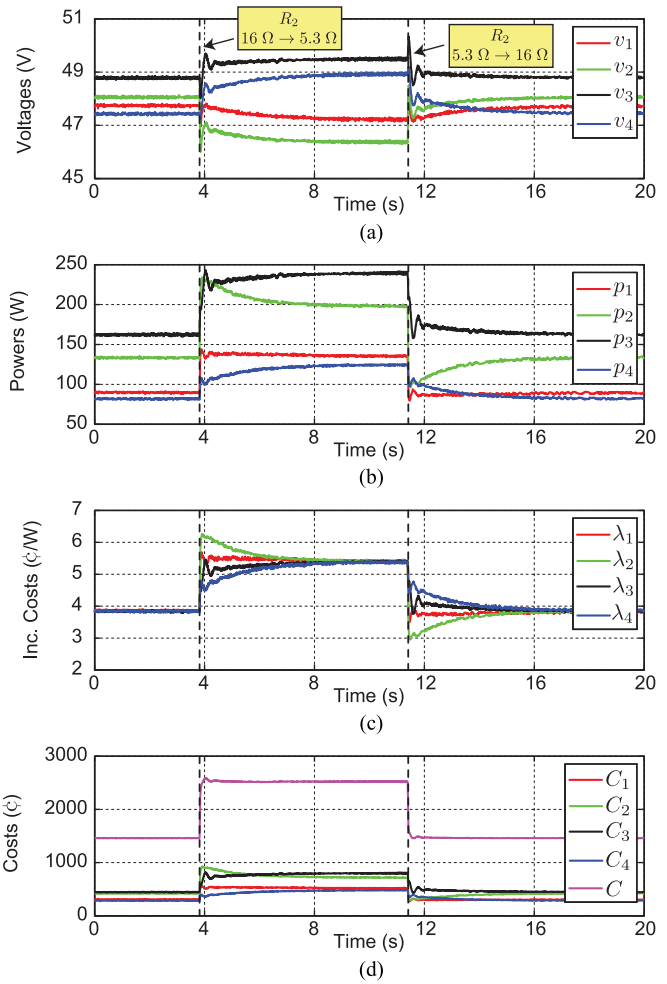

Fig. 14. Steep load change. (a) Voltages. (b) Powers. (c) Incremental costs. (d) Costs.

communication weights of the network change from 1.25 to 2.5 (red asterisks show the poles at $a_{ij} = 1.25$). As seen, the system has two real poles on the OLHP and they move toward origin as the communication weights increase.

B. *Performance Verification Under Normal Operation*

The controller performance upon activation is verified in Fig. 13. First, the proposed control system is disabled, and the rated voltage of the microgrid is assigned as the set points of all converters. Fig. 13(a) shows that all the output voltages are initially regulated at 48 V. At $t = 6.2$ s, the proposed controller is activated to adjust the output voltages, which accordingly changes the output powers so that all the λ_is reach a consensus at 3.85 ¢/W after a short transient time [see Fig. 13(a)–(c)]. It can be seen in Fig. 13(d) that the total cost C, which is the sum of four individual costs C_i, becomes less upon activating the proposed controller.

Next, the controller efficacy, in a case of a steep load change, is verified. As seen in Fig. 14, the controller is performing well at the beginning, where a consensus on λ_is is established at 3.85 ¢/W. The load of the second converter, R_2, is changed

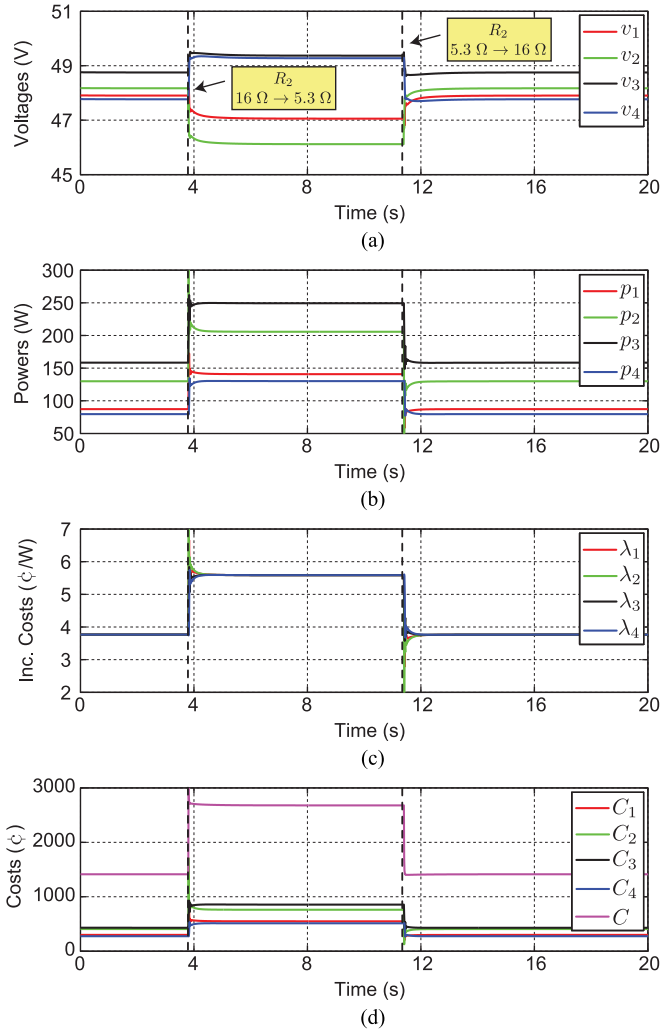

Fig. 15. Simulation results for the same study of Fig. 14. (a) Voltages. (b) Powers. (c) Incremental costs. (d) Costs.

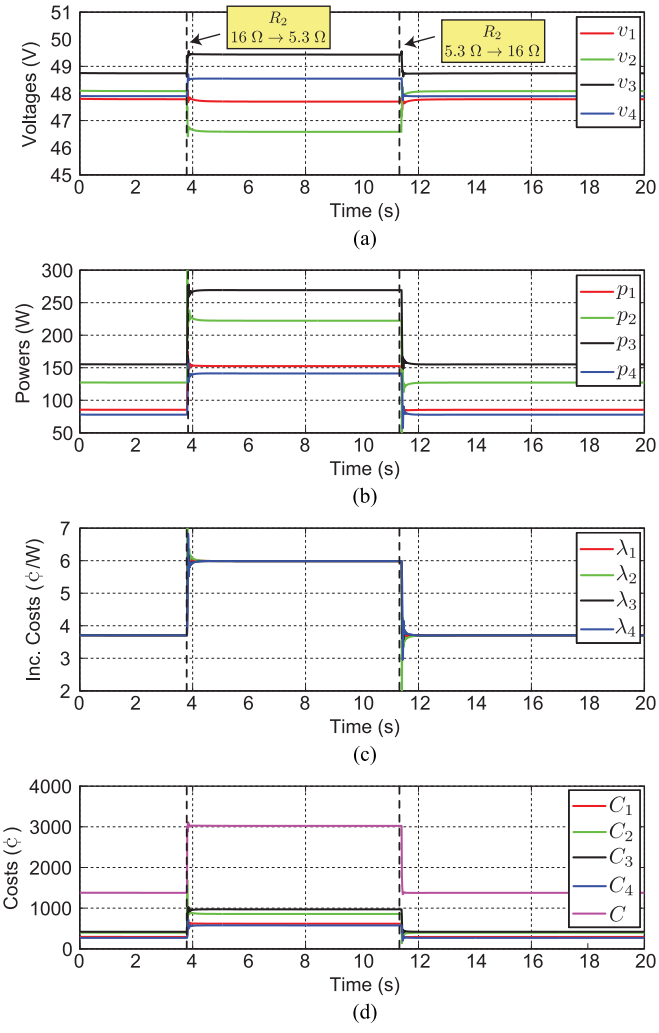

Fig. 16. Simulation results for the same study of Fig. 14 with a battery added at Bus 4. (a) Voltages. (b) Powers. (c) Incremental costs. (d) Costs.

from 16 to 5.3 Ω at $t = 3.8$ s. This increased load requires more generation to maintain the equality constraint in (6). Accordingly, as seen in Fig. 14(a), the average output voltage is maintained at the global reference voltage, 48 V. Therefore, the output powers of all of the sources are increased so that the λ_is reach a new consensus at 5.4 ¢/W after a short transient [see Fig. 14(b) and (c)]. Given the increased total power, the total cost has increased too, but it is still the minimum cost for the new loading configuration [see Fig. 14(d)]. As shown in Fig. 14(a), the load R_2 is reduced from 5.3 to 16 Ω at $t = 11.4$ s, which decreases the total power demand. Accordingly, the voltages go back to their initial values, the output powers are decreased to maintain the equality constraint in (6), and λ_is reach a consensus at their initial values. The simulation results for the same test are presented in Fig. 15 and show an acceptable match between the simulation and experimental results.

To verify the controller performance in the presence of storage units, the previous simulation setup is modified by adding a battery at Bus 4. The battery is modeled by an internal voltage source of 48 V and an internal resistance of 0.5 Ω. As seen in Fig. 16, the battery provides (absorbs) energy for (from) the microgrid and decreases (increases) the total generation cost, when the voltage at Bus 4 is less (more) than 48 V. In addition, the incremental cost matching is established during all the times.

Next, the controller performance, when a source reaches its maximum generation limit, is studied. The third converter had reached 240 W in Fig. 14(b). In the current study, the third converter output is limited to 200 W. Once R_2 is changed from 16 to 5.3 Ω at $t = 5.4$ s, all the output powers must increase to maintain the equality constraint between the generation and consumption. However, p_3 cannot exceed its maximum limit and is limited to 200 W [see Fig. 17(b)]. Accordingly, λ_3 cannot join the consensus with the other three λ_is and is regulated at its maximum value, $\lambda_{3,\max} = \beta_3 + 2\gamma_3 p_{3,\max} = 4.6$ ¢/W, while the other λ_is reach a consensus at 5.8 ¢W. The new consensus value is larger than that of the previous study because the three participating sources must generate more power to compensate for the limitation imposed on the third converter. In addition, Fig. 17(d) shows that the total generation cost is slightly greater than that of the previous study (i.e., 2548 ¢ compared to 2518 ¢). As seen in Fig. 17, the communication among three participating agents for optimizer can

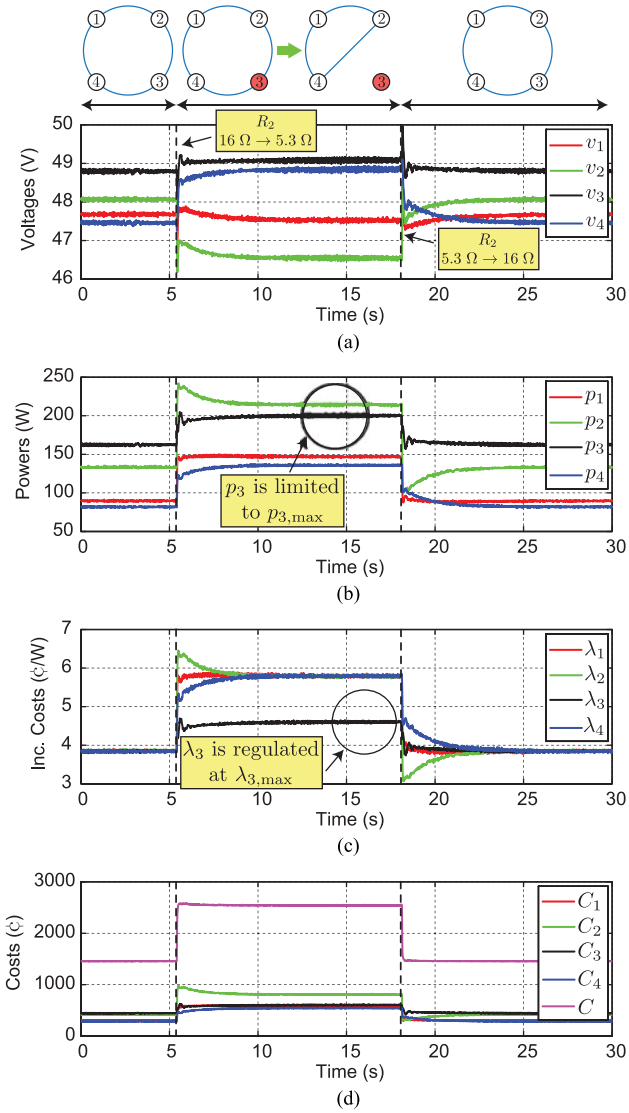

Fig. 17. One source reaches its maximum generation limit. (a) Voltages. (b) Powers. (c) Incremental costs. (d) Costs.

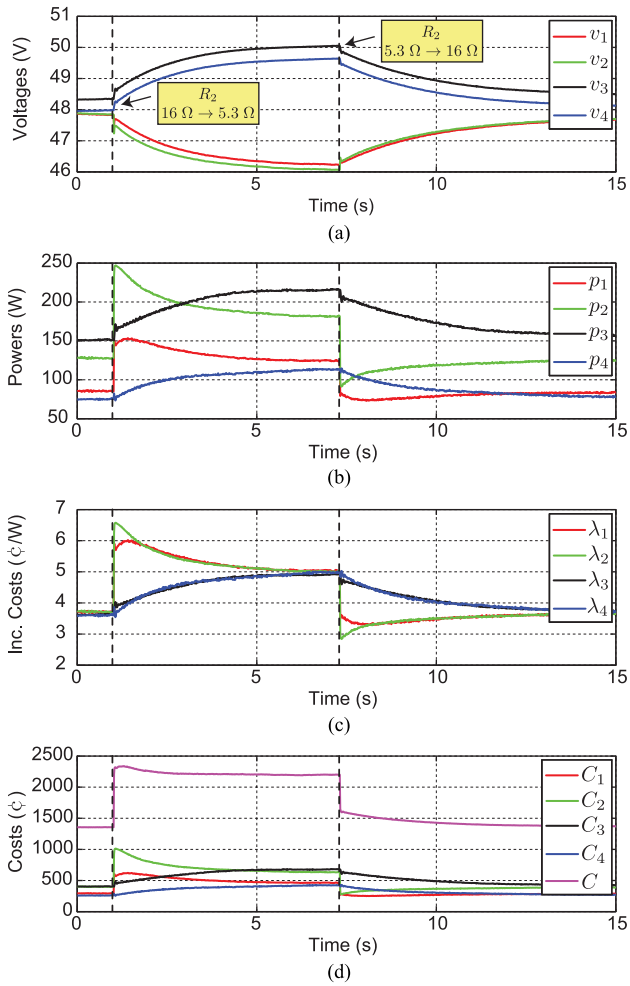

Fig. 18. Controller performance in presence of constant power loads. (a) Voltages. (b) Powers. (c) Incremental costs. (d) Costs.

be represented with a modified graph with three nodes. It should be noted that the communication graph used for both optimization and voltage regulation remains the same graph with four nodes. However, since the incremental cost of source 3 is not passed to its neighbors, the communication of the agents for optimization is represented by a graph with three nodes. The load resistance is changed back to 16 Ω at $t = 18.1$ s, which causes all the states (e.g., voltages, currents, powers) to go back to their initial conditions.

Next study verifies the controller performance in presence of controllable loads. To this end, one of the resistive loads in the system, i.e., R_1, is replaced with an electronic load set on constant power mode with 200 W. The results are reported in Fig. 18, where one of the resistive loads, i.e., R_2 is changed from 16 Ω to 5.3 Ω at $t = 1$ s, while the controller is enabled. As seen in Fig. 18(c), incremental cost matching among sources, which is established before the load change, is established again after the load change, which accordingly modifies the source voltages. The resistive load is changed back from 5.3 to 16 Ω at $t = 7.2$ s, which causes the controllers to bring back all the incremental costs to their initial values.

The controller performance, when the cost function is changed, is reported in Fig. 19. The proposed controller is operating under the default condition, until $t = 3.9$ s when one of the cost coefficients of source 1, i.e., γ_1, is changed from 0.017 to 0.011 ¢/W^2. As the generation cost of source 1 is decreased, its incremental cost λ_1 drops instantly [see Fig. 19(c)]. Therefore, by changing the output voltages, source 1 increases its output, while the other three sources decrease theirs to maintain the generation–consumption balance [see Fig. 19(b)]. Accordingly, the other three λ_is reach a new consensus with λ_1 at 3.5 ¢/W. As seen in Fig. 19(d), the total cost is reduced from 1463 to 1396 ¢. As shown in Fig. 19(a), the cost function coefficient of source 1 is changed back to its initial value at $t = 16.7$ s, which brings back the system to its initial condition.

Next, the effects of changes in communication links characteristic, i.e., channel bandwidth and delay, on the controller performance are studied. At the beginning of each experiment, the controller in disabled (see shaded parts in Figs. 20 and 21) and, then, becomes active. As shown in Fig. 20, a wide range

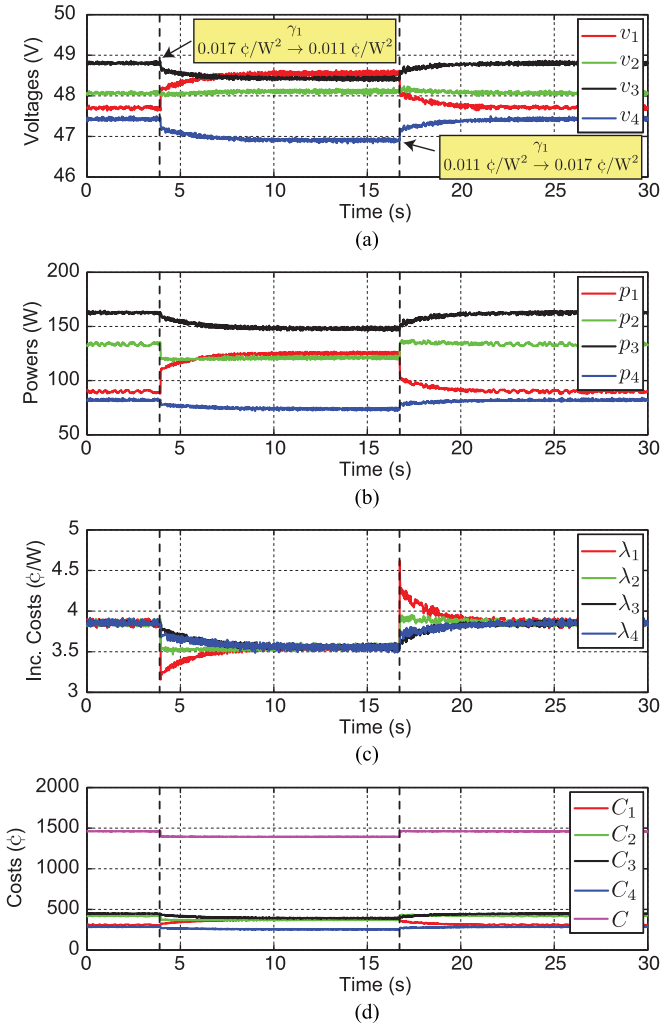

Fig. 19. Controller performance with the change in the cost function. (a) Voltages. (b) Powers. (c) Incremental costs. (d) Costs.

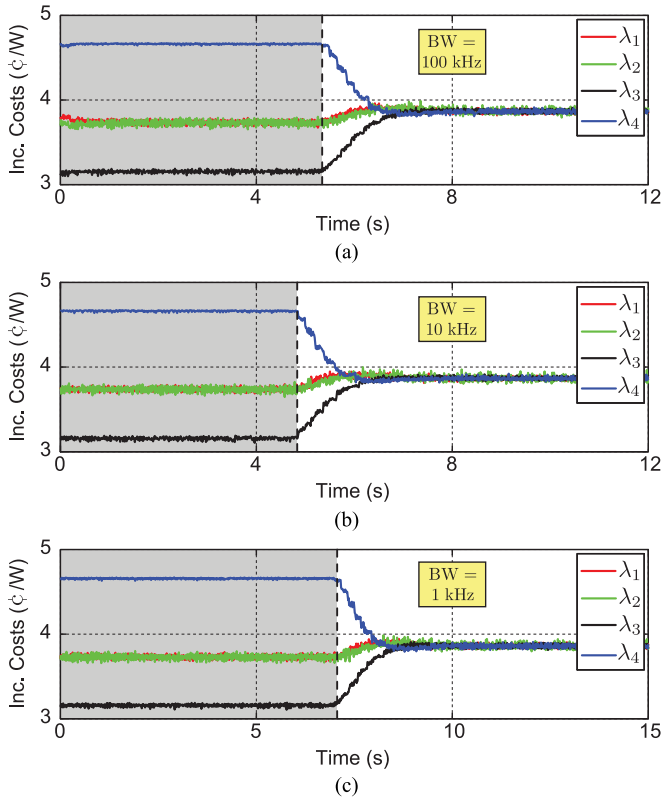

Fig. 20. Effect of bandwidth of communication channel on controller performance.

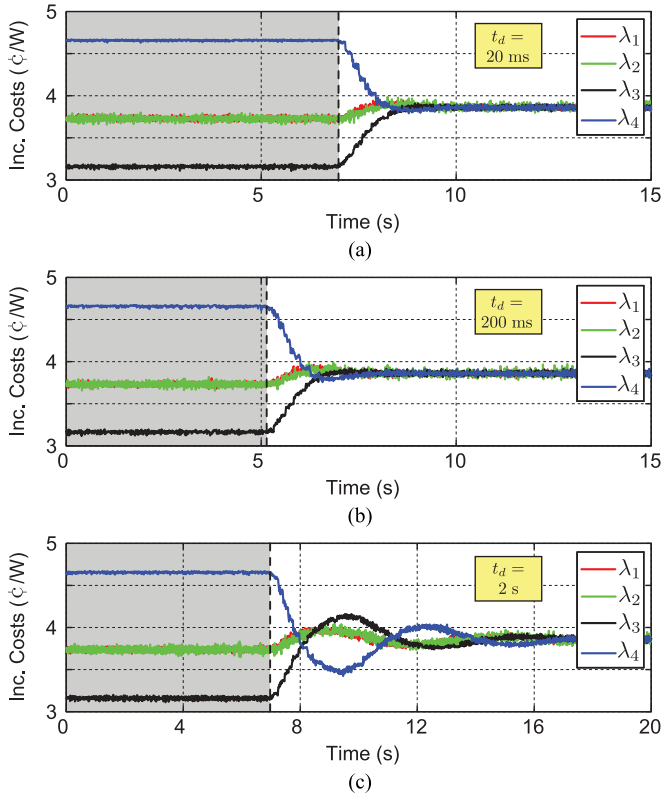

Fig. 21. Effect of communication delay on controller performance.

of communication bandwidths is selected in the experiments, i.e., 100, 10, and 1 kHz, while the delay time is set to 20 ms. Comparing the results of Fig. 20, no significant difference can be observed. The controller performs well in load sharing for all different bandwidths. Three different delay times, i.e., 0.02, 0.2, and 2 s, are selected to study the delay effect, while the bandwidth is set to 1 kHz (see Fig. 21). No significant difference can be observed between performances for delay times of 20 and 200 ms. In both cases, the incremental cost matching is established after short-time dynamics, preceding controller activation. However, in the case of $t_d = 2$ s, the transients take much longer to decay. However, the overshoots/undershoots remain intact and the controller performs well at the steady state. Overall, it can be concluded that the controller performance has immunity to delay times as long as 200 ms and bandwidths as low as 1 kHz. Therefore, common communication protocols, such as WiFi and UWB, are possible choices. Interested readers are encouraged to read more details on communication links characteristics in distributed systems in [79], [87], and [88].

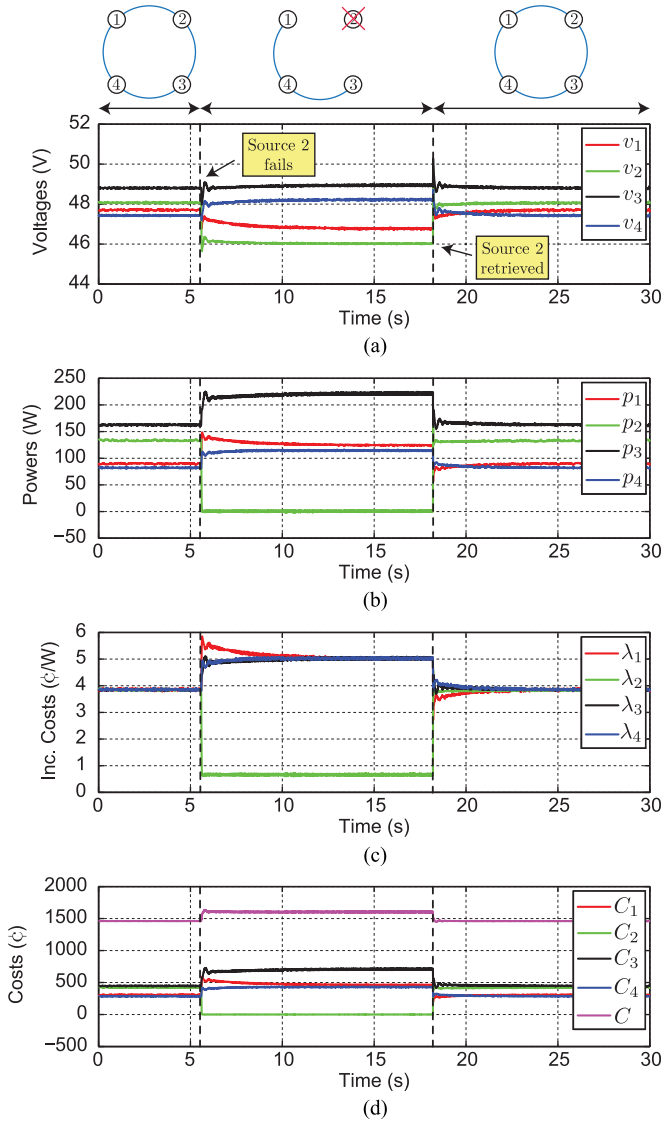

Fig. 22. Controller response to the source failure. (a) Voltages. (b) Powers. (c) Incremental costs. (d) Costs.

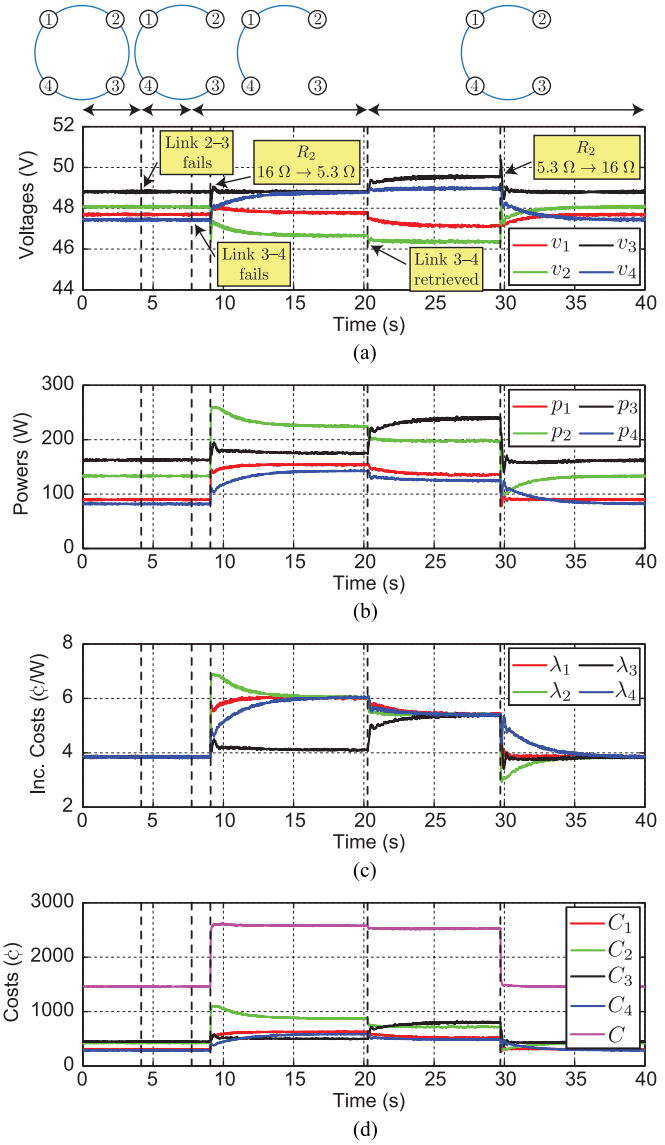

Fig. 23. Controller response to the link failure. (a) Voltages. (b) Powers. (c) Incremental costs. (d) Costs.

C. Performance Validation Under Faults

The plug-and-play capability of the proposed controller is verified next when the second converter has failed and recovered. As shown in Fig. 22(a), the system is operating under normal condition until $t = 5.6$ s, when the second converter has failed and the communication links of Node 2 are disabled, which modifies the communication graph (see Fig. 22). The voltage controller regulates the average voltage of the other three sources at 48 V. The remaining three sources increase their generation to compensate for the failure of Source 2. Accordingly, their incremental costs increase and reach a new consensus at 5 ¢//W. Then, at $t = 18.2$ s, the failed source is recovered, which establishes its communication links, and reaches a new consensus at the initial value of 3.85 ¢/W by changing the output voltages.

The last study verifies the controller performance when the communication links are compromised. As seen in Fig. 23(a), the microgrid is operating under normal conditions until $t = 4.1$ s, when the communication link 2-3 fails, although the graphical connectivity remains intact and the controller remains functional. Then, at $t = 7.75$ s, the communication link 3-4 is also disconnected, which violates graphical connectivity and isolates Node 3. All converters, however, maintain their previous output voltages. However, once R_2 is changed from 16

TABLE I
ELECTRICAL SPECIFICATIONS OF THE PROTOTYPED MICROGRID

Item	Value
Rated voltage	48 V
Distribution line resistance	1 Ω
Distribution line inductance	112 μH
Distribution line capacitance	44 nF
Converters' rating	400 W

TABLE II
ELECTRICAL PARAMETERS OF BUCK CONVERTERS

Converter	$v_{\rm in}$ (V)	$L_{\rm out}$ (mH)	$C_{\rm out}$ (mF)	R (Ω)
Converter 1	100	3.10	2.10	23
Converter 2	90	3.11	2.12	16
Converter 3	80	3.09	2.07	29
Converter 4	70	3.12	2.19	18

TABLE III
COST FUNCTION COEFFICIENTS OF SOURCES

Source	α (¢)	β (¢/W)	γ (¢/W^2)
Source 1	100	0.80	0.017
Source 2	120	0.65	0.012
Source 3	85	0.60	0.010
Source 4	90	0.90	0.018

to 5.3 Ω at $t = 9.1$ s, the third converter, which is graphically isolated, cannot adapt its voltage for the new loading condition. The other three sources adjust their voltages to increase their generation and meet the additional demand. The three remaining sources bring their incremental costs to a consensus, which is suboptimal as expected when the graphical connectivity is lost. Link 3-4 is retrieved at $t = 20.3$ s, which establishes the graphical connectivity and leads to global consensus among λ_is. Accordingly, the generation cost in decreased and the optimal operating point is achieved. It can be seen that the proposed cooperative controller performs well so long as the communication graph remains connected. Finally, at $t = 29.7$ s, R_2 is changed back to 16 Ω and the system returns to its initial condition.

VIII. CONCLUSION

A distributed coordination and optimization paradigm is investigated to coordinate source voltages and optimally share power among sources within a dc microgrid. The proposed method solves an economic dispatch problem to optimize the power sharing among sources by matching the incremental costs of neighbor sources. A voltage regulator takes care of the generation–demand equality constraint by regulating the average voltage of the sources, while an optimizer matches their incremental costs. Both controllers are implemented in a fully distributed fashion, and generate voltage correction terms which are added to the rated voltage and provide the voltage set point of dc–dc converters. The optimizer is modified to take care of generation-limit inequality constraints by excluding the source from the incremental-cost consensus protocol. A dynamic model of the proposed controller is extracted, and the steady-state analysis is performed to validate the desired performance of the proposed controller. The experimental results verify the efficacy of the proposed controller in power sharing and under physical and cyber fault conditions.

APPENDIX

Electrical specifications of the prototyped microgrid are tabulated in Tables I. In addition, Electrical parameters of the buck converters and the cost function coefficients of the sources are tabulated in Tables II and III, respectively. The coupling gain c is 20. The diagonal matrices of PI controllers of the voltage regulator are

$$\mathbf{H}_{\rm P} = 0.01 \times \begin{bmatrix} 5 & 0 & 0 & 0 \\ 0 & 4 & 0 & 0 \\ 0 & 0 & 5 & 0 \\ 0 & 0 & 0 & 6 \end{bmatrix}, \quad \mathbf{H}_{\rm I} = \begin{bmatrix} 1.2 & 0 & 0 & 0 \\ 0 & 1.3 & 0 & 0 \\ 0 & 0 & 1.1 & 0 \\ 0 & 0 & 0 & 1.4 \end{bmatrix} \tag{60}$$

and those of the optimizer are

$$\mathbf{G}_{\rm P} = \begin{bmatrix} 1.1 & 0 & 0 & 0 \\ 0 & 1 & 0 & 0 \\ 0 & 0 & 1.2 & 0 \\ 0 & 0 & 0 & 1 \end{bmatrix}, \quad \mathbf{G}_{\rm I} = \begin{bmatrix} 7 & 0 & 0 & 0 \\ 0 & 7.4 & 0 & 0 \\ 0 & 0 & 6.6 & 0 \\ 0 & 0 & 0 & 7 \end{bmatrix}. \tag{61}$$

REFERENCES

[1] [Online]. Available: http://energy.gov/sites/prod/files/EAC%20Presentation%20-%20OE%20Microgrid%20R%26D%20Initiative%202011%20-%20Smith.pdf, 2011.

[2] A. Kwasinski and C. N. Onwuchekwa, "Dynamic behavior and stabilization of dc microgrids with instantaneous constant-power loads," *IEEE Trans. Power Electron.*, vol. 26, no. 3, pp. 822–834, Mar. 2011.

[3] T. Dragicevic, X. Lu, J. C. Vasquez, and J. M. Guerrero, "DC microgrids—Part I: A review of control strategies and stabilization techniques," *IEEE Trans. Power Electron.*, vol. 31, no. 7, pp. 4876–4891, Jul. 2016.

[4] T. Dragicevic, X. Lu, J. C. Vasquez, and J. M. Guerrero, "DC microgrids—Part II: A review of power architectures, applications and standardization issues," *IEEE Trans. Power Electron.*, vol. 31, no. 5, pp. 3528–3549, May 2016.

[5] M. Ebad and W. M. Grady, "An approach for assessing high-penetration PV impact on distribution feeders," *Elect. Power Syst. Res.*, vol. 133, pp. 347–354, Apr. 2016.

[6] J. Xiao, P. Wang, and L. Setyawan, "Implementation of multiple-slack-terminal dc microgrids for smooth transitions between grid-tied and islanded states," *IEEE Trans. Smart Grid*, vol. 7, no. 1, pp. 273–281, Jan. 2016.

[7] D. Wu, F. Tang, T. Dragicevic, J. Guerrero, and J. Vasquez, "Coordinated control based on bus-signaling and virtual inertia for islanded dc microgrids," *IEEE Trans. Smart Grid*, vol. 6, no. 6, pp. 2627–2638, Nov. 2015.

[8] S. Konar and A. Ghosh, "Interconnection of islanded dc microgrids," in *Proc. IEEE PES Asia-Pacific Power Energy Eng. Conf.*, Nov. 2015, pp. 1–5.

[9] S. Liu, W. Zhu, Y. Cheng, and B. Xing, "Modeling and small-signal stability analysis of an islanded dc microgrid with dynamic loads," in *Proc. IEEE 15th Int. Conf. Environ. Elect. Eng.*, Jun. 2015, pp. 866–871.

[10] T. Vu, S. Paran, F. Diaz, T. Meyzani, and C. Edrington, "Model predictive control for power control in islanded dc microgrids," in *Proc. IEEE 41st Annu. Conf. Ind. Electron. Soc.*, Nov. 2015, pp. 1610–1615.

[11] M. Tucci, S. Riverso, J. C. Vasquez, J. M. Guerrero, and G. Ferrari-Trecate, "Voltage control of dc islanded microgrids: A decentralized scalable approach," in *Proc. IEEE 54th Annu. Conf. Decision Control*, Dec. 2015, pp. 3149–3154.

[12] A. Nobrega Tahim, D. Pagano, E. Lenz, and V. Stramosk, "Modeling and stability analysis of islanded dc microgrids under droop control," *IEEE Trans. Power Electron.*, vol. 30, no. 8, pp. 4597–4607, Aug. 2015.

[13] M. Kumar, S. Srivastava, and S. Singh, "Control strategies of a dc microgrid for grid connected and islanded operations," *IEEE Trans. Smart Grid*, vol. 6, no. 4, pp. 1588–1601, Jul. 2015.

[14] S. Moayedi and A. Davoudi, "Distributed tertiary control of dc microgrid clusters," *IEEE Trans. Power Electron.*, vol. 31, no. 2, pp. 1717–1733, Feb. 2016.

[15] J. M. Guerrero, J. C. Vasquez, J. Matas, L. G. de Vincuña, and M. Castilla, "Hierarchical control of droop-controlled ac and dc microgrids – A general approach toward standardizationn," *IEEE Trans. Ind. Electron.*, vol. 58, no. 1, pp. 158–172, Jan. 2011.

[16] C. Jin, P. Wang, J. Xiao, Y. Tang, and F. H. Choo, "Implementation of hierarchical control in dc microgrids," *IEEE Trans. Ind. Electron.*, vol. 61, no. 8, pp. 4032–4042, Aug. 2014.

[17] M. Ebad and B. M. Song, "Accurate model predictive control of bidirectional dc-dc converters for dc distributed power systems," in *Proc. IEEE Power Energy Soc. Gen. Meeting*, Jul. 2012, pp. 1–8.

[18] V. Nasirian, S. Moayedi, A. Davoudi, and F. Lewis, "Distributed cooperative control of dc microgrids," *IEEE Trans. Power Electron.*, vol. 30, no. 4, pp. 2288–2303, Apr. 2015.

[19] L. Xu and D. Chen, "Control and operation of a dc microgrid with variable generation and energy storage," *IEEE Trans. Power Del.*, vol. 26, no. 4, pp. 2513–2522, Oct. 2011.

[20] H. Kakigano, Y. Miura, and T. Ise, "Low-voltage bipolar-type dc microgrid for super high quality distribution," *IEEE Trans. Power Electron.*, vol. 25, no. 12, pp. 3066–3075, Dec. 2010.

[21] D. Chen and L. Xu, "Autonomous dc voltage control of a dc microgrid with multiple slack terminals," *IEEE Trans. Power Syst.*, vol. 27, no. 4, pp. 1897–1905, Nov. 2012.

[22] L. Gan and S. H. Low, "Optimal power flow in direct current networks," *IEEE Trans. Power Electron.*, vol. 29, no. 6, pp. 2892–2904, Nov. 2014.

[23] M. B. Shadmand and R. S. Balog, "Multi-objective optimization and design of photovoltaic-wind hybrid system for community smart dc microgrid," *IEEE Trans. Smart Grid*, vol. 5, no. 5, pp. 2635–2643, Sep. 2014.

[24] L. Meng, T. Dragicevic, J. M. Guerrero, and J. C. Vasquez, "Dynamic consensus algorithm based distributed global efficiency optimization of a droop controlled dc microgrid," in *Proc. IEEE Int. Energy Conf.*, May 2014, pp. 1276–1283.

[25] S. Anand, B. G. Fernandes, and J. M. Guerrero, "Distributed control to ensure proportional load sharing and improve voltage regulation in low-voltage dc microgrids," *IEEE Trans. Power Electron.*, vol. 28, no. 4, pp. 1900–1913, Apr. 2013.

[26] X. Lu, J. M. Guerrero, K. Sun, and J. C. Vasquez, "An improved droop control method for dc microgrids based on low bandwidth communication with dc bus voltage restoration and enhanced current sharing accuracy," *IEEE Trans. Power Electron.*, vol. 29, no. 4, pp. 1800–1812, Apr. 2014.

[27] P.-H. Huang, P.-C. Liu, W. Xiao, and M. S. El Moursi, "A novel droop-based average voltage sharing control strategy for dc microgrids," *IEEE Trans. Smart Grid*, vol. 6, no. 3, pp. 1096–1106, May 2015.

[28] H. Behjati, A. Davoudi, and F. Lewis, "Modular dc-dc converters on graphs: Cooperative control," *IEEE Trans. Power Electron.*, vol. 29, no. 12, pp. 6725–6741, Dec. 2014.

[29] S. Moayedi, V. Nasirian, F. Lewis, and A. Davoudi, "Team-oriented load sharing in parallel dc-dc converters," *IEEE Trans. Ind. Appl.*, vol. 51, no. 1, pp. 479–490, Jan./Feb. 2015.

[30] C.-L. Su, K.-L. Lin, and C.-J. Chen, "Power flow and generator-converter schemes studies in ship MVDC distribution systems," *IEEE Trans. Ind. Appl.*, vol. 52, no. 1, pp. 50–59, Jan. 2016.

[31] J. Shi, R. Amgai, and S. Abdelwahed, "Modelling of shipboard medium-voltage direct current system for system level dynamic analysis," *IET Elect. Syst. Transp.*, vol. 5, no. 4, pp. 156–165, Dec. 2015.

[32] S. Sudhoff *et al.*, "A reduced scale naval dc microgrid to support electric ship research and development," in *Proc. IEEE Elect. Ship Technol. Symp.*, Jun. 2015, pp. 464–471.

[33] H. Li, W. Li, M. Luo, A. Monti, and F. Ponci, "Design of smart MVDC power grid protection," *IEEE Trans. Instrum. Meas.*, vol. 60, no. 9, pp. 3035–3046, Sep. 2011.

[34] A. Trias and J. Marin, "The holomorphic embedding loadflow method for dc power systems and nonlinear dc circuits," *IEEE Trans. Circuits Syst. I, Reg. Papers*, vol. 63, no. 2, pp. 322–333, Feb. 2016.

[35] G. Reed, B. Grainger, A. Sparacino, and Z.-H. Mao, "Ship to grid: Medium-voltage dc concepts in theory and practice," *IEEE Power Energy Mag.*, vol. 10, no. 6, pp. 70–79, Nov. 2012.

[36] J. Ciezki and R. Ashton, "Selection and stability issues associated with a navy shipboard dc zonal electric distribution system," *IEEE Trans. Power Del.*, vol. 15, no. 2, pp. 665–669, Apr. 2000.

[37] C.-L. Su, K.-L. Lin, and C.-J. Chen, "Power flow and generator-converter schemes studies in ship MVDC distribution systems," *IEEE Trans. Ind. Appl.*, vol. 52, no. 1, pp. 50–59, Jan. 2016.

[38] N. Doerry, "Naval power systems: Integrated power systems for the continuity of the electrical power supply." *IEEE Electrific. Mag.*, vol. 3, no. 2, pp. 12–21, Jun. 2015.

[39] *IEEE Recommended Practice for Electric Installations on Shipboard*, IEEE Std 45-2002 (Revision of IEEE Std 45-1998), Oct. 2002, pp. 1–272.

[40] B. Zahedi and L. Norum, "Modeling and simulation of all-electric ships with low-voltage dc hybrid power systems," *IEEE Trans. Power Electron.*, vol. 28, no. 10, pp. 4525–4537, Oct. 2013.

[41] C.-L. Su, K.-L. Lin, and C.-J. Chen, "Power flow and generator-converter schemes studies in ship MVDC distribution systems," *IEEE Trans. Ind. Appl.*, vol. 52, no. 1, pp. 50–59, Jan. 2016.

[42] X. Roboam, B. Sareni, and A. Andrade, "More electricity in the air: Toward optimized electrical networks embedded in more-electrical aircraft," *IEEE Ind. Electron. Mag.*, vol. 6, no. 4, pp. 6–17, Dec. 2012.

[43] P. Magne, B. Nahid-Mobarakeh, and S. Pierfederici, "General active global stabilization of multiloads dc-power networks," *IEEE Trans. Power Electron.*, vol. 27, no. 4, pp. 1788–1798, Apr. 2012.

[44] A. Griffo and J. Wang, "Large signal stability analysis more electric aircraft power systems with constant power loads," *IEEE Trans. Aerosp. Electron. Syst.*, vol. 48, no. 1, pp. 477–489, Jan. 2012.

[45] H. Zhang, F. Mollet, C. Saudemont, and B. Robyns, "Experimental validation of energy storage system management strategies for a local dc distribution system of more electric aircraft," *IEEE Trans. Ind. Electron.*, vol. 57, no. 12, pp. 3905–3916, Dec. 2010.

[46] P. Magne, B. Nahid-Mobarakeh, and S. Pierfederici, "Active stabilization of dc microgrids without remote sensors for more electric aircraft," *IEEE Trans. Ind. Appl.*, vol. 49, no. 5, pp. 2352–2360, Sep. 2013.

[47] [Online]. Available: http://energy.gov/sites/prod/files/2015/03/f20/DC_Microgrid_Scoping_Study_LosAlamos-Mar2015.pdf, 2015.

[48] M. Sechilariu, B. Wang, and F. Locment, "Power management and optimization for isolated dc microgrid," in *Proc. Int. Symp. Power Electron., Elect. Drives, Autom. Motion*, Jun. 2014, pp. 1284–1289.

[49] N. Ekneligoda and W. Weaver, "Game theoretic optimization of dc microgrids without a communication infrastructure," in *Proc. Clemson Univ. Power Syst. Conf.*, Mar. 2014, pp. 1–6.

[50] L. Zubieta, "Power management and optimization concept for dc microgrids," in *Proc. IEEE 1st Int. Conf. DC Microgrids*, Jun. 2015, pp. 81–85.

[51] J. Ma, F. He, and Z. Zhao, "Line loss optimization based OPF strategy by hierarchical control for dc microgrid," in *Proc. IEEE Energy Convers. Congr. Expo.*, Sep. 2015, pp. 6212–6216.

[52] T. Vu, S. Paran, T. El Mezyani, and C. Edrington, "Real-time distributed power optimization in the dc microgrids of shipboard power systems," in *Proc. IEEE Elect. Ship Technol. Symp.*, Jun. 2015, pp. 118–122.

[53] M. Hossain and H. Ginn, "Real-time distributed coordination of power electronic converters for optimization of dc shipboard distribution systems," in *Proc. IEEE Elect. Ship Technol. Symp.*, Jun. 2015, pp. 19–26.

[54] A. J. Wood and B. F. Wollenberg, *Power Generation, Operation and Control*. New York, NY, USA: Wiley, 1996.

[55] R. Bronson and G. Naadimuthu, *Operations Research*. New York, NY, USA: McGraw-Hill, 1997.

[56] I. U. Nutkani, W. Peng, P. C. Loh, and F. Blaabjerg, "Cost-based droop scheme for dc microgrid," in *Proc. IEEE Energy Convers. Congr. Expo.*, Sep. 2014, pp. 765–769.

[57] A. C. Luna, N. L. Diaz, L. Meng, M. Graells, J. C. Vasquez, and J. M. Guerrero, "Generation-side power scheduling in a grid-connected dc microgrid," in *Proc. 1st IEEE Int. Conf. DC Microgrids*, Jun. 2015, pp. 327–332.

[58] L. T. Dos Santos, M. Sechilariu, and F. Locment, "Day-ahead microgrid optimal self-scheduling: Comparison between three methods applied to isolated dc microgrid," in *Proc. 40th IEEE Annu. Conf. Ind. Electron.*, Oct. 2014, pp. 2010–2016.

[59] G. Carpinelli, A. Bracale, and P. Caramia, "Plug-and-play control and optimization in microgrids," in *Proc. 12th Int. Conf. Environ. Elect. Eng.*, May 2013, pp. 573–578.

[60] D. Chen, L. Xu, and L. Yao, "DC voltage variation based autonomous control of dc microgrids," *IEEE Trans. Power Del.*, vol. 28, no. 2, pp. 637–648, Apr. 2013.

[61] A. Khorsandi, M. Ashourloo, and H. Mokhtari, "A decentralized control method for a low-voltage dc microgrid," *IEEE Trans. Energy Convers.*, vol. 29, no. 4, pp. 793–801, Dec. 2014.

[62] Y. Gu, X. Xiang, W. Li, and X. He, "Mode-adaptive decentralized control for renewable dc microgrid with enhanced reliability and flexibility," *IEEE Trans. Power Electron.*, vol. 29, no. 9, pp. 5072–5080, Sep. 2014.

[63] V. Nasirian, A. Davoudi, F. L. Lewis, and J. M. Guerrero, "Distributed adaptive droop control for dc distribution systems," *IEEE Trans. Energy Convers.*, vol. 29, no. 4, pp. 944–956, Dec. 2014.

[64] L. Meng, T. Dragicevic, J. M. Guerrero, and J. C. Vasquez, "Dynamic consensus algorithm based distributed global efficiency optimization of

a droop controlled dc microgrid," in *Proc. IEEE Int. Energy Conf.*, May 2014, pp. 1276–1283.
[65] L. Meng, T. Dragicevic, J. Guerrero, and J. Vasquez, "Optimization with system damping restoration for droop controlled dc-dc converters," in *Proc. IEEE Energy Convers. Congr. Expo.*, Sep. 2013, pp. 65–72.
[66] Q. Shafiee, T. Dragicevic, J. C. Vasquez, and J. M. Guerrero, "Hierarchical control for multiple dc-microgrids clusters," *IEEE Trans. Energy Conv.*, vol. 29, no. 4, pp. 922–933, Dec. 2014.
[67] L. Meng, *et al.*, "Distributed voltage unbalance compensation in islanded microgrids by using dynamic-consensus-algorithm," *IEEE Trans. Power Electron.*, vol. 31, no. 1, pp. 827–838, Jan. 2016.
[68] H. Kakigano, Y. Miura, and T. Ise, "Distribution voltage control for dc microgrids using fuzzy control and gain-scheduling technique," *IEEE Trans. Power Electron.*, vol. 28, no. 5, pp. 2246–2258, May 2013.
[69] N. L. Diaz, T. Dragicevic, J. C. Vasquez, and J. M. Guerrero, "Intelligent distributed generation and storage units for dc microgrids: A new concept on cooperative control without communications beyond droop control," *IEEE Trans. Smart Grid*, vol. 5, no. 5, pp. 2476–2485, Sep. 2014.
[70] C. Li, S. K. Chaudhary, T. Dragicevic, J. C. Vasquez, and J. M. Guerrero, "Power flow analysis for dc voltage droop controlled dc microgrids," in *Proc. 11th Int. Multi-Conf. Syst. Signals Devices*, Feb. 2014, pp. 1–5.
[71] F. Dorfler, J. W. Simpson-Porco, and F. Bullo, "Breaking the hierarchy: Distributed control and economic optimality in microgrids," *arXiv preprint arXiv:1401.1767v2*, Dec. 2014.
[72] E. Dall'Anese, S. V. Dhople, and G. B. Giannakis, "Photovoltaic inverter controllers seeking ac optimal power flow solutions," *arXiv preprint arXiv:1501.00188v2*, Apr. 2015.
[73] F. Dorfler, J. W. Simpson-Porco, and F. Bullo, "Plug-and-play control and optimization in microgrids," in *Proc. 53rd IEEE Annu. Conf. Decision Control*, Dec. 2014, pp. 211–216.
[74] X. Zhang and A. Papachristodoulou, "Distributed dynamic feedback control for smart power networks with tree topology," in *Proc. Am. Control Conf.*, Jun. 2014, pp. 1156–1161.
[75] L. Chen, C. Zhao, and N. Li, "Connecting automatic generation control and economic dispatch from an optimization view," *IEEE Trans. Control Netw. Syst.*, 2015, doi: 10.1109/TCNS.2015.2459451, to be published.
[76] X. Ma and N. Elia, "A distributed continuous-time gradient dynamics approach for the active power loss minimizations," in *Proc. 51st Annu. Allerton Conf. Commun. Control Comput. Power Electron. Conf. Expo.*, Oct. 2013, pp. 100–106.
[77] A. Bidram, A. Davoudi, and F. L. Lewis, "A multiobjective distributed control framework for islanded ac microgrids," *IEEE Trans. Ind. Informat.*, vol. 10, no. 3, pp. 1785–1798, Aug. 2014.
[78] Z. Qu, *Cooperative Control of Dynamical Systems: Applications to Autonomous Vehicles*. New York, NY, USA: Springer-Verlag, 2009.
[79] R. Olfati-Saber and R. M. Murray, "Consensus problems in networks of agents with switching topology and time-delays," *IEEE Trans. Autom. Control*, vol. 49, no. 9, pp. 1520–1533, Sep. 2004.
[80] S. Moayedi and A. Davoudi, "Distributed cooperative load sharing in parallel dc-dc converters," in *Proc. 29th IEEE Annu. Appl. Power Electron. Conf. Expo.*, Mar. 2014, pp. 2907–2912.
[81] G. Binetti, A. Davoudi, F. L. Lewis, D. Naso, and B. Turchiano, "Distributed consensus-based economic dispatch with transmission losses," *IEEE Trans. Power Syst.*, vol. 29, no. 4, pp. 1711–1720, Jul. 2014.
[82] V. Loia and A. Vaccaro, "Decentralized economic dispatch in smart grids by self-organizing dynamic agents," *IEEE Trans. Syst. Man Cybern. A., Syst. Humans*, vol. 44, no. 4, pp. 397–408, Apr. 2014.
[83] C. Jin, P. Wang, J. Xiao, Y. Tang, and F. H. Choo, "Implementation of hierarchical control in dc microgrids," *IEEE Trans. Ind. Electron.*, vol. 61, no. 8, pp. 4032–4042, Aug. 2014.
[84] S. Augustine, M. K. Mishra, and N. Lakshminarasamma, "Adaptive droop control strategy for load sharing and circulating current minimization in low-voltage standalone dc microgrid," *IEEE Trans. Sustain. Energy*, vol. 6, no. 1, pp. 132–141, Jan. 2015.
[85] J. Schonberger, R. Duke, and S. D. Round, "DC-bus signaling: A distributed control strategy for a hybrid renewable nanogrid," *IEEE Trans. Ind. Electron.*, vol. 53, no. 5, pp. 1453–1460, Oct. 2006.
[86] K. Sun, L. Zhang, Y. Xing, and J. M. Guerrero, "A distributed control strategy based on dc bus signaling for modular photovoltaic generation systems with battery energy storage," *IEEE Trans. Power Electron.*, vol. 26, no. 10, pp. 3032–3045, Oct. 2011.
[87] N. Amelinaand A. Fradkov, "Consensus problem in stochastic network systems with switched topology, noise and delay," in *Proc. 12th IEEE Int. Conf. Netw.*, Jan. 2013, pp. 118–124.
[88] S. Kar and J. M. F. Moura, "Distributed consensus algorithms in sensor networks with imperfect communication: Link failures and channel noise," *IEEE Trans. Signal Process.*, vol. 57, no. 1, pp. 355–369, Jan. 2009.

Seyedali Moayedi (S'12) received the B.Sc. and M.Sc. degrees from the Sharif University of technology, Tehran, Iran, in 2007 and 2009, respectively, and the Ph.D. degree from University of Texas, Arlington, TX, USA, in 2015, all in electrical engineering.

He is currently a Postdoctoral Researcher and an Adjunct Professor with the University of Texas at Arlington. His research interests include design, modeling, and control of power electronics, electric drive systems, and distributed control systems.

Ali Davoudi (S'04–M'11–SM'15) received the Ph.D. degree in electrical and computer engineering from the University of Illinois, Urbana-Champaign, Urbana, IL, USA, in 2010.

He is currently an Assistant Professor with the Department of Electrical Engineering, University of Texas, Arlington, TX, USA. He was with Solar Bridge Technologies, Champaign, IL; Texas Instruments Inc., Rochester, MN; and Royal Philips Electronics, Rosemont, IL. His research interests include various aspects of modeling and control of power electronics and finite-inertia power systems.

Dr. Davoudi is an Associate Editor for the IEEE TRANSACTIONS ON INDUSTRY APPLICATIONS, IEEE TRANSACTIONS ON TRANSPORTATION ELECTRIFICATION, and IEEE TRANSACTIONS ON ENERGY CONVERSION. He has received 2014 Ralph H. Lee Prize Paper Award from the IEEE TRANSACTIONS ON INDUSTRY APPLICATIONS, the Best Paper Award from the 2015 IEEE International Symposium on Resilient Control Systems, and the 2014–2015 Best Paper Award from the IEEE TRANSACTIONS ON ENERGY CONVERSION.